Geol. Mag. **149** (*1*), *2012, pp. 1–18. © Cambridge University Press 2011*
doi:10.1017/S001675681100015X

Petrogenesis of Cenozoic mafic–ultramafic alkaline lavas from the Tigris volcanic field, NE Syria

ABDEL-FATTAH M. ABDEL-RAHMAN* & NANCY A. LEASE

Department of Geology, American University of Beirut, P.O. Box 11-0236, Beirut, Lebanon, and Ministère de l'Agriculture, des Pêcheries et de l'Alimentation, Sainte-Foy, Québec, G1R 4×6, Canada

(*Received* 24 May 2010; *accepted* 5 January 2011; *first published online* 4 March 2011)

Abstract – Mafic–ultramafic Quaternary lava flows form the Tigris volcanic field (covering 1750 km^2) at the northeastern tip of Syria and extend into Turkey. This volcanic field occurs between the Euphrates graben and the Bitlis–Zagros collision suture that forms the boundary between the Arabian and Eurasian plates. The rocks are made up of labradorite, clinopyroxene, olivine and opaque phases. The Tigris lavas are compositionally restricted to basanites and alkali basalts, having a narrow range of major element compositions (SiO_2, 42.2–48.2 wt %; MgO, 5.7–9.0 wt %, with Mg numbers ranging from 0.51 to 0.62; TiO_2, 1.7–3.2 wt %), and are alkaline in nature. The rocks are enriched in HFS elements such as Zr (119–231 ppm), Nb (14–43 ppm) and Y (17–22 ppm). The REE patterns are strongly fractionated ($(La/Yb)_N = 10.6$), indicative of a garnet-bearing source. The $^{143}Nd/^{144}Nd$ isotopic compositions range from 0.512803 to 0.512908, and $^{87}Sr/^{86}Sr$ from 0.70327 to 0.70403 ($\varepsilon_{Nd} = 3.2–5.3$) suggesting strong affinities to ocean island basalts. Modelling using a variety of mantle source materials and different degrees of partial melting indicates that the magma was produced by a small degree of batch partial melting (F = 1.5 %) of a primitive, garnet-lherzolite fertile mantle source. The overall petrological/chemical nature supports this interpretation. Shear heating at the base of the lithospheric mantle of the northern boundary of the Arabian plate, caused by a change in plate motion as the Arabian plate moved in a more easterly direction during the Plio-Quaternary, could represent a possible source of the heat necessary for partial fusion and magma generation. Adiabatic decompression and melting represents a more likely process for the generation of the Tigris magma. Elemental ratios such as K/P (4.6), La/Ta (12), La/Nb (0.90), Nb/Y (1.22) and Th/Nb (0.09) indicate that the magma was subjected to minimal crustal contamination.

Keywords: Tigris region, geochemistry, Nd–Sr isotopes, petrogenetic modelling, Bitlis–Zagros suture, alkaline basalt, Arabian plate.

1. Introduction

Major problems in understanding the cause of volcanism remain unresolved, and a number of questions in connection with the genesis of basaltic magmas in general have not yet been fully answered. The chemical signatures of alkali basalts that are related to various tectonic settings such as oceanic or continental rifting, transtensional regimes or hot spots of plume or non-plume origin, and the nature of the mantle source material, whether it is dominated by recycled oceanic or continental crust, or by recycled sedimentary components, of a primitive, depleted, then later metasomatized origin, whether related to lithospheric or sub-lithospheric depths, and the processes associated with melting and migration of melt, are among the more hotly debated topics on the subject. Some of these issues will be discussed through this case study on the mafic–ultramafic Tigris lavas of northeastern Syria, which provides insight into the magmatic processes associated with the youngest phases of Cenozoic volcanism in the Middle East.

Volcanism occurring at the northeasternmost tip of Syria near its borders with Iraq and Turkey (Figs 1, 2) is represented by the Tigris volcanic field, which extends further north across the border into Turkey. This volcanic field occurs within a tectonically active region and represents an example of mafic rocks that form a prime constituent of the crustal segment of the Middle East. As the petrology and geochemistry of the Tigris volcanic field have not been previously investigated, we aim to provide petrological, chemical and isotopic data on this volcanic field, provide constraints on its mantle source and propose a petrogenetic model for its lavas. The data will also be used to shed light on the tectonic regime of magma emplacement in the context of the regional geodynamic framework.

*Author for correspondence: arahman@aub.edu.lb

2. Overview of the regional tectonic framework

The Tigris volcanic field occurs between the Bitlis–Zagros collisional suture to the north and east, and a tensional-related fracture system (the Euphrates graben) to the south (Fig. 2a, b). This volcanic field represents the northern segment of the Middle East Cenozoic volcanic province (Fig. 1). The latter consists of large, discontinuous volcanic exposures extending from Sinai, Jordan and Israel, to Lebanon, Syria and Turkey (Dubertret, 1955; Mouty *et al*. 1992; Shaw *et al*. 2003; Abdel-Rahman & Nassar, 2004; Weinstein

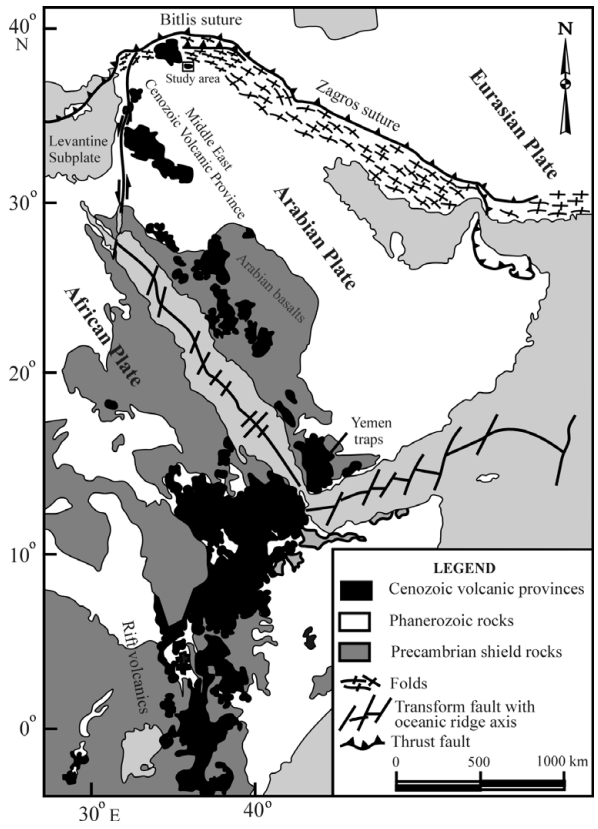

Figure 1. Regional geological map showing the distribution of the various Cenozoic volcanic provinces in east Africa, Arabia and the Middle East. The area of study is located to the south of the Bitlis–Zagros suture.

et al. 2006; Lustrino & Sharkov, 2006; Lease & Abdel-Rahman, 2008). As a result of such a major phase of Cenozoic volcanism, some other extensive volcanic provinces were developed further south in east Africa (mostly Ethiopia and Kenya), in Yemen and in Arabia (Mohr, 1983; White & McKenzie, 1989; Camp & Roobol, 1992; Camp, Roobol & Hooper, 1992; Baker, Thirlwall & Menzies, 1996; Bertrand *et al*. 2003; Furman *et al*. 2006). The study of Furman *et al*. (2004) showed that the Quaternary mafic lavas of northern Kenya were derived from mixtures of plume and ambient mantle sources. The Tertiary mafic lavas of Kenya were interpreted to reflect isotopically distinct plume heads beneath Tanzania and Afar that are derived from the chemically heterogeneous South African superplume (Furman *et al*. 2006). The Cenozoic lava flows in Ethiopia that are thought to be clearly related to the East African rift system were interpreted to have been developed in association with the Afar plume (Barberi *et al*. 1975; Mohr, 1983; Hart *et al*. 1989; Stewart & Rogers, 1996; Barrat *et al*. 1998; Pik *et al*. 1999; George & Rogers, 2002). In fact, Ebinger & Sleep (1998) indicated that Cenozoic magmatism throughout east Africa resulted from the impact of a single plume. Baker *et al*. (1997, 1998) demonstrated that the mafic lavas of western Yemen were produced in response to small amounts of lithospheric extension that were metasomatized and hydrated by the Afar plume.

The Cenozoic continental flood basalts of Saudi Arabia were interpreted to have occurred in two distinct phases (Camp & Roobol, 1989, 1992; Camp, Roobol & Hooper, 1992): phase one (30 to 20 Ma) of tholeiitic to transitional lavas was related to passive mantle upwelling during extension of the Red Sea basin, and phase two (12 Ma to Recent) that produced transitional to strongly alkalic lavas, was related to active mantle upwelling facilitated by minor continental extension. White & McKenzie (1989) and Camp & Roobol (1992) concluded that the source of upwelling is either a mantle plume centrally located beneath the West Arabian Swell, or an elongated and extended lobe of hot asthenosphere emanating from the Ethiopian mantle plume. In sharp contrast, the Afar plume of Ethiopia is thought not to have been channelled northwestwards beneath the Arabian plate, and has played no role in producing the Cenozoic volcanic field of Jordan (Shaw *et al*. 2003). These Jordanian alkali basalts and basanites were formed in response to a phase of lithospheric extension.

According to Baldridge *et al*. (1991), Miocene basaltic magmatism in Sinai was developed in association with the opening of the Red Sea. Garfunkel (1989) described the 'Cover' Cenozoic basalts, which are located in southeastern Galilee and in the southern Golan Heights, as mostly alkaline basalts of intraplate character and ocean island basalt (OIB) affinities, and proposed that the Jordan Valley depression could have acted as a route for magma ascent. Weinstein *et al*. (2006) proposed that basanites and basalts of the southern Golan–Galilee region have two mantle sources (a dehydrated garnet-bearing amphibole peridotite and amphibole–garnet-bearing pyroxenite veins) occurring at lithospheric depths and that they were formed by dehydration and partial melting of an originally isotopically uniform reservoir.

The Pliocene alkali basalts of northern Lebanon, according to Abdel-Rahman & Nassar (2004), were thought to have erupted during an episode of localized extension, which occurred particularly at the junction between the Dead Sea–Ghab transform and the Yammouneh restraining bend (i.e. in a transtensional tectonic regime). Mouty *et al*. (1992) presented preliminary geochronological data on Cenozoic volcanism in Syria, in which they produced whole-rock K–Ar ages ranging from 23.5 to 1.5 Ma. They demonstrated that there was a large gap (between 16 and 8 Ma) in Cenozoic volcanic activity, and interpreted this to correspond with the interval between the two stages of spreading of the Red Sea–Dead Sea rift system, with magmatism being associated with left-lateral movements along the Dead Sea rift. Lustrino & Sharkov (2006) indicated that much of the Neogene volcanic activity in western Syria was concentrated near the Dead Sea transform fault system: they concluded that the origin of the lavas in that region reflects a strong lithospheric control on the loci of partial melting, which developed as a result of mantle decompression formed as a consequence of the transition from strongly

https://doi.org/10.1017/S001675681100015X Published online by Cambridge University Press

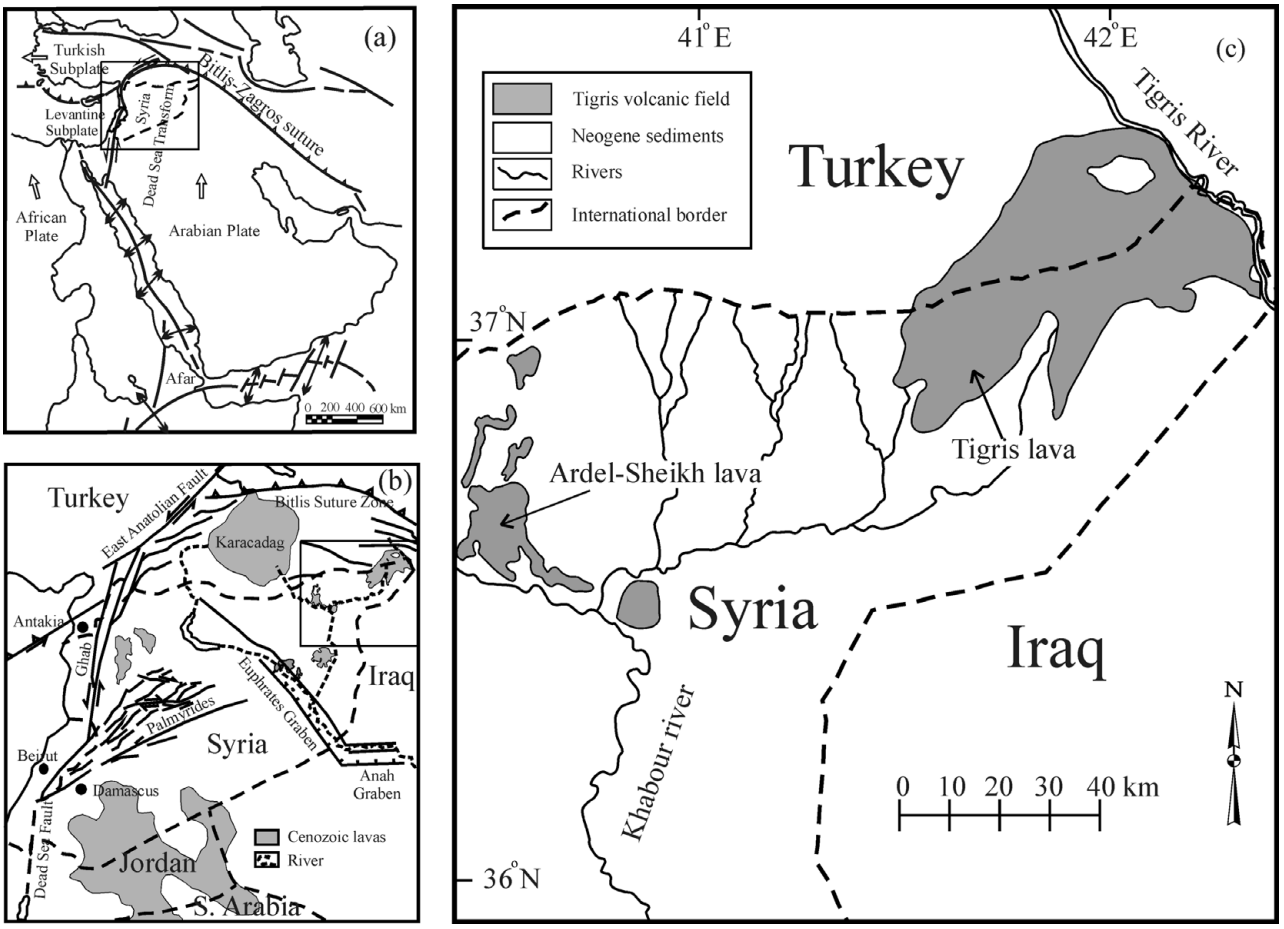

Figure 2. Geological and tectonic maps showing (a) the main tectonic elements in the Middle East (square outlines map 2b), (b) the area of study and some of the structural elements (square outlines map 2c), and (c) simplified geological map of northeastern Syria at its borders with Turkey and Iraq showing locations of the various exposures within the Tigris volcanic field (after Ponikarov, 1967).

compressive to transtensional stresses. They found no evidence to relate volcanic activity there to any mantle plume. Lease & Abdel-Rahman (2008) proposed that the Plio-Quaternary Euphrates mafic lavas of eastern Syria are of within-plate alkaline nature, exhibit strong OIB affinities, and were erupted along reactivated deep-seated fractures that were developed beneath the Euphrates basin. The Karacadag volcanic plateau of southern Turkey is covered largely by Late Cenozoic lavas, with K–Ar ages ranging from Late Pliocene to Recent, as reported in Pearce *et al*. (1990) and Notsu *et al*. (1995). Pearce *et al*. (1990) concluded that these transitional to alkaline mafic lavas were derived from the mantle lithosphere of the Arabian continent, which had been enriched by small volumes of asthenospheric melts.

3. The geological context

Volcanism of the Arabian foreland, directly south of the Bitlis suture zone, includes lavas of northeastern Syria (the Tigris volcanic field) and the Karacadag lavas in Turkey. The Tigris field consists of several exposures in the Ardel-Sheikh and Tigris regions (Fig. 2), within which the volcanic rocks in the Syrian part cover an area of about 1750 km^2. These volcanic exposures contain lava flows ranging in age from Plio-Quaternary to Recent. The manifestations of volcanism are in the form of fissure eruptions and small shield volcanoes. The Tigris volcanic field is located between latitudes 36° 30′ and 37° 30′ N and longitudes 40° 20′ and 42° 20′ E, within northeastern Syria (Fig. 2c). The Tigris lava flows were erupted onto undeformed Neogene and Quaternary sediments. Regional mapping of Dubertret (1955) showed the Neogene and Quaternary volcanic rocks of Syria and Lebanon to be fissure-type eruptions. He stated that lava ascended along re-activated, as well as Recent fault planes, forming voluminous flows.

The Tigris volcanic field is made up of basaltic lava flows, with minor pyroclastic flows. The lavas are mainly composed of phyric varieties (olivine basalts), forming fine-grained, massive rocks with variable degrees of vesicularity. The flows form plateaus typical of shield-type volcanoes, and the lower unit in some of the volcanic piles is topped by craters with lava flows and associated pyroclastic materials, reflecting mixed effusive and explosive activity. Lava flows in the Ardel-Sheikh area occur either at the extension of a zone of NE-trending faults, or in volcanic exposures controlled by the intersection between localized N–S-trending fissures and the extension of NE-trending

https://doi.org/10.1017/S001675681100015X Published online by Cambridge University Press

regional faults. The thickness of lava flow exposures in the Ardel-Sheikh area ranges from 5 m to a maximum of 20 m. Columnar jointed flows, as well as sub-vertical injections of basaltic dykes into Neogene sedimentary host rocks have been observed. These dykes are made up of highly vesicular basalt, with some large vesicles that range from 5 to 15 cm across. Within the Tigris region, lava flow exposures range typically from 10 to 20 m thick, but reaching over 100 m thick at the axial zone of the plateau; the Tigris River forms the eastern boundary of this volcanic plateau. Massive to vesicular porphyritic basalt, containing olivine and clinopyroxene phenocrysts, is the most common lithological variety. Blocky basalt in this region exhibits large blocks in the order of one cubic metre. More recent volcanic activity is indicated by the superposition of lava and scoria cones on the earlier Plio-Quaternary flows (e.g. Ponikarov, 1967).

The Tigris volcanic field that occurs on the northern flank of the Arabian plate is situated near major tectonic features: the Bitlis–Zagros suture zone to the north and east, the Euphrates graben (a tensional-related fracture system) in the south, and the left-lateral East Anatolian fault as well as the left-lateral Dead Sea–Ghab transform fault system occurring further to the west (Fig. 2a, b). Sawaf *et al*. (1993) indicated that the Euphrates graben/fault system was developed by extension/transtension following a period of extensive uplift and erosion during Jurassic and Early Cretaceous time. According to Giannerini *et al*. (1988), a change in plate motion occurred during the Plio-Quaternary, when the Arabian plate rotated to the northeast. The left-lateral Dead Sea–Ghab transform fault system has been active since the end of the Miocene (Lyberis *et al*. 1992), and permits the northward movement of the Arabian plate and its collision with Eurasia along the Bitlis–Zagros suture (Fig. 2a, b).

4. Analytical procedures

4.a. Major and trace element analyses

Twenty representative whole-rock samples from the Tigris volcanic field have been analysed for major- and trace elements at the Activation Laboratories (ACTLABS) in Ancaster, Canada. The samples were mixed with a mixture of lithium metaborate/lithium tetraborate and fused. The molten mixture was poured into a 5 % nitric acid solution and shaken for approximately 30 minutes until dissolved. The samples were run for major oxides on a combination simultaneous and sequential Thermo Jarrell-Ash Enviro II ICP. Calibration was achieved using a combination of CANMET and USGS reference materials. Loss on ignition (LOI) was determined by heating powdered samples for 50 minutes. The analytical precision, as calculated from 20 replicate analyses of one sample, is better than 1 % for most major elements and better than 5 % for most trace elements.

4.b. Rare earths, hafnium and tantalum

Analyses for the rare earth elements (REEs), hafnium and tantalum were also conducted at the Activation Laboratories. Solutions of the fused samples, prepared as above, were spiked with three internal standards to cover the entire mass range. These were further diluted and introduced into a Perkin Elmer-SCIEX Elan 6000 ICP-MS using a proprietary sample introduction methodology. The fusion process ensures measurement of total metals (particularly for elements like REEs in resistate phases; this may not be the case for acid digestions, particularly for heavy rare earth elements (HREEs) and other elements contained in refractory minerals like zircon, sphene or monazite). Detection limits and reagent blanks are generally about 10 % of chondrite values. The primitive mantle values used for normalization are those of Sun & McDonough (1989).

4.c. Isotopes

The Sr and Nd isotopic analyses were conducted at McMaster University, Ontario, Canada. Before commencing the chemical procedures, sample powders were leached in 6M HCl for several hours in order to remove any traces of secondary strontium. Nd and Sr were separated in cation exchange columns; the separation was followed by purification in a second separation column according to the method of Richard, Shimizu & Allègre (1976). The solution of Nd was mounted on double filaments and measured on a VG Isolab-54 mass spectrometer with multiple collectors in dynamic mode. During the course of the study, the La Jolla Nd standard gave $^{143}Nd/^{144}Nd = 0.51185$. The average precision of repetitions was $\pm$ 0.000015 (2σ). The solution of Sr was mounted on a single filament and measured by a VG Isomass-354 with multiple collectors. The Sr isotopes were normalized for fractionation to $^{86}Sr/^{88}Sr = 0.1194$, related to a value of 0.710241 for the NBS-987 standard. The average precision of repetitions was $\pm$ 0.00002 (2σ).

5. Petrography of the Tigris volcanic rocks

The various lithologies are largely phyric, consisting mainly of olivine and clinopyroxene $\pm$ minor plagioclase phenocrysts, occurring within microcrystalline to cryptocrystalline groundmass materials. The latter is made up mainly of plagioclase laths, minute crystals of clinopyroxene and olivine, as well as opaque phases. Textures in these volcanic rocks vary from porphyritic, glomeroporphyritic and rarely aphyric, to ophitic, sub-ophitic, vesicular, intersertal and pilotaxitic.

Labradorite (50 to 55 vol. % of the rock) forms crystals that range in size from tiny microlites to large prisms, occurring mostly as groundmass material in the form of microlaths, and rarely as rectangular microphenocrysts or phenocrysts. Micro-inclusions of apatite needles are occasionally present in some plagioclase crystals. Clinopyroxene forms about 35 vol. %

https://doi.org/10.1017/S001675681100015X Published online by Cambridge University Press

of the rock, occurring both as a phenocryst and as a groundmass phase. Clinopyroxene is rarely twinned and occurs as anhedral to subhedral crystals, sometimes showing complex and sector zoning. Complex zonation observed may be due to simultaneous crystallization of some clinopyroxene with labradorite. Olivine (10 to 15 vol. %) occurs both as subhedral to euhedral, large, equant, occasionally skeletal phenocrysts, and as minute anhedral groundmass crystals. The olivine phenocrysts are generally fresh, but in some rocks olivine is partially altered to iddingsite. Corroded and embayed olivine phenocrysts are observed in many samples. Inclusions of Cr-rich spinel are occasionally present in some olivine crystals. Titan-magnetite, ilmenite and magnetite, occurring as small cubes or acicular needles within the groundmass, represent the main opaque phases present in the Tigris volcanic rocks.

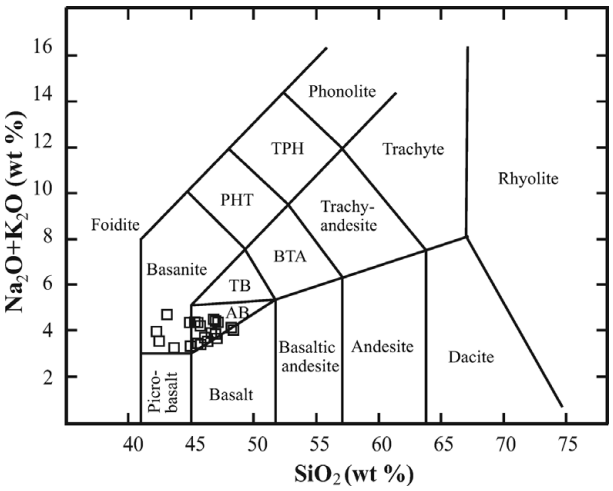

Figure 3. Total alkali–silica (TAS) diagram (after Le Bas & Streckeisen, 1991); data points occupy the fields of basanite and alkali basalt (AB). TPH – tephriphonolite; PHT – phonotephrite; TB – trachybasalt; BTA – basaltic trachyandesite.

6. Geochemistry

6.a. Major and trace element geochemistry

Data on whole-rock major and trace elements for 20 representative samples from the Tigris volcanic field are given in Table 1. Based on their silica contents, the investigated rocks are ultrabasic to basic, as they have low silica values (42.2 to 48.2 wt % SiO_2). In general, these rocks exhibit narrow major element compositional ranges: 12.6–15.9 wt % Al_2O_3, 5.7–9.0 wt % MgO, 12.6–14.5 wt % Fe_2O_3 (as total iron), 7.8–11.5 wt % CaO and 1.7–3.2 wt % TiO_2 (Table 1). The Mg numbers (= molar Mg/(Mg + Fe^{2+}), assuming an Fe^{3+}/Fe^{2+} ratio of 0.2) range from 0.51 to 0.62, with an average of 0.58, thus suggesting that the magma may have undergone a degree of olivine and clinopyroxene fractionation. Using the diagram of Le Bas & Streckeisen (1991), the investigated rocks are classified as basanites and alkali basalts (Fig. 3). Rocks of the Tigris volcanic field have a relatively narrow trace element compositional range: Cr = 87–334 ppm, V = 188–275 ppm, Sr = 357–827 ppm, Ba = 104–377 ppm and Rb = 5–16 ppm (Table 1), and are generally enriched in the high-field-strength (HFS) elements such as Zr (119–231 ppm), Y (17–22 ppm) and Nb (14–43 ppm). Averages of some elemental ratios in the Tigris lavas, such as La/Nb (1.11), Zr/Nb (6.96) and Rb/Nb (0.41), along with trace element concentrations are somewhat similar to those in some OIB lavas (Sun & McDonough, 1989; Weaver, 1991).

Data points of the Tigris volcanic field, as plotted on variation diagrams of selected major elements versus Zr (Fig. 4), indicate that P_2O_5, TiO_2 and CaO increase gradually with increasing Zr, whereas alkalis and total iron (as Fe_2O_3) remain somewhat constant. Variations of selected trace elements versus Zr indicate that most trace elements, such as Sr, Y and Nb, show a gradual increase with increasing Zr (Fig. 4). Since Zr and Y are incompatible in the main fractionating phases of basaltic magmas (olivine, pyroxene and plagioclase), the Zr/Y ratio is not normally affected by moderate amounts of fractional crystallization. The variation of Zr/Y with Zr or with FeO could be used to illustrate petrogenetic processes such as fractional crystallization or partial melting. As Zr is more incompatible in mantle phases than Y (Nicholson & Latin, 1992), the Zr/Y ratio tends to be higher when the degree of melting is small. Thus, basalts produced by small degrees of partial melting at high pressures have high Zr/Y ratios (and high concentrations of FeO): the Zr/Y ratios in the Tigris rocks are quite high, varying from 6.5 to 11.6. Also, the linear positive variations of Zr/Y, which decrease gradually with decreasing Zr, suggest that partial melting processes have played a significant role in producing the range of magma compositions observed (see Section 7). Trace element data suggest that the Tigris rocks display the geochemical characteristics of within-plate lavas (e.g. Pearce & Norry, 1979; Meschede, 1986).

6.b. The rare earth elements

The concentration of the rare earth elements (REEs) for 20 representative samples of the Tigris volcanic field are given in Table 2, and their primitive mantle-normalized REE patterns are presented in Figure 5a. In general, the investigated lavas are enriched in the REEs, with the sum of REEs ranging from 80 to 188 ppm. The REE patterns are uniform, parallel to subparallel and show that the REEs are strongly fractionated ($(La/Yb)_N = 10.6$), as the light rare earth elements (LREEs) are significantly enriched compared to the HREEs (Fig. 5a). Two of the basanite samples (numbers SF-134 and SF-27) that possess some of the lowest SiO_2 contents (42.2 and 43.0 wt % SiO_2) exhibit the highest LREE concentrations. This feature is most likely the result of differences in the degrees of partial melting of the mantle source rock; it is not due to contamination (see Section 7). Enrichment in

https://doi.org/10.1017/S001675681100015X Published online by Cambridge University Press

Table 1. Major and trace element composition (in wt % and ppm, respectively) of representative samples of the Tigris volcanic field, northeastern Syria

Sample	AS07	AS17	AS37	AS57	AS67	AS77	AS104	AS124	AS184	AS194	TG17	TG27	TG37	TG47	TG144	TG154	TG164	TG174	SF134	SF27	
Long.	40°42′ 42″ E	40°37′ 25″ E	40°41′ 36″ E	40°38′ 06″ E	40°27′ 21″ E	40°33′ 54″ E	40°36′ 37″ E	40°32′ 54″ E	40°28′ 40″ E	40°24′ 08″ E	42°07′ 57″ E	42°12′ 08″ E	42°08′ 45″ E	41°52′ 31″ E	41°51′ 53″ E	42°10′ 14″ E	42°07′ 11″ E	42°08′ 31″ E	40°34′ 03″ E	40°34′ 13″ E	
Lat.	36°34′ 50″ N	36°35′ 32″ N	36°34′ 53″ N	36°35′ 24″ N	36°43′ 19″ N	36°42′ 00″ N	36°34′ 28″ N	36°41′ 32″ N	36°36′ 21″ N	36°38′ 30″ N	37°12′ 03″ N	37°16′ 35″ N	37°09′ 08″ N	36°59′ 15″ N	36°58′ 52″ N	37°07′ 10″ N	37°07′ 54″ N	37°08′ 49″ N	36°50′ 02″ N	36°47′ 50″ N	Ave.
SiO_2	45.67	43.59	45.69	45.49	44.82	45.50	46.60	45.33	42.42	44.86	46.89	46.02	48.17	46.72	46.78	48.21	46.27	47.02	42.19	43.02	45.56
TiO_2	2.42	2.16	2.31	2.38	2.54	2.76	2.36	2.68	2.45	2.41	2.00	2.03	2.15	1.99	2.50	1.65	1.86	1.87	3.18	3.23	2.35
Al_2O_3	14.72	13.79	15.03	14.82	13.95	15.63	15.89	15.64	13.66	14.12	15.07	14.94	15.47	14.22	14.58	15.18	13.80	14.69	12.80	12.63	14.53
Fe_2O_3*	13.44	13.32	13.84	13.91	13.75	12.93	12.63	12.75	13.43	13.55	14.45	13.70	13.37	13.46	13.04	13.12	13.72	14.22	13.80	14.12	13.53
MgO	7.50	8.74	8.02	7.88	8.42	5.69	6.81	5.72	8.02	9.01	6.14	7.96	6.37	8.48	6.41	8.16	8.93	7.44	8.35	8.13	7.61
MnO	0.17	0.17	0.16	0.17	0.18	0.17	0.16	0.16	0.17	0.16	0.19	0.17	0.17	0.16	0.16	0.17	0.17	0.18	0.17	0.17	0.17
CaO	10.52	11.51	9.29	9.96	9.72	11.46	10.67	11.03	11.54	10.00	8.83	9.13	9.35	9.12	9.17	8.54	8.31	7.84	10.90	10.01	9.85
Na_2O	3.33	2.55	2.64	2.67	3.24	3.28	3.11	3.23	2.59	2.54	3.13	2.78	3.27	3.47	3.17	3.28	2.81	2.96	2.80	3.20	3.00
K_2O	0.91	0.71	0.73	0.79	1.12	1.09	0.83	1.13	0.94	0.77	0.73	0.92	0.85	1.02	1.26	0.78	0.76	0.72	1.14	1.48	0.934
P_2O_5	0.37	0.32	0.33	0.33	0.46	0.47	0.36	0.48	0.47	0.43	0.27	0.34	0.34	0.28	0.38	0.24	0.35	0.26	0.62	0.60	0.385
LOI	0.64	3.48	1.57	1.5	1.13	1.23	0.81	0.85	2.72	2.78	2.33	1.84	0.30	0.86	2.20	0.42	1.40	1.42	3.13	2.91	1.676
Total	99.67	100.33	99.61	99.91	99.33	100.18	100.24	99.00	98.39	100.63	100.01	99.82	99.81	99.78	99.67	99.75	98.38	98.62	99.08	99.48	99.64
Sc	25	23	26	25	23	24	24	24	21	22	25	21	25	19	17	22	20	24	19	19	22.40
V	242	226	252	241	235	261	247	275	241	238	243	210	244	188	194	211	205	231	261	261	235.30
Cr	281	324	334	295	265	87	228	105	230	294	291	305	211	283	158	285	252	271	307	304	255.50
Ni	186	260	229	212	236	54	171	77	266	264	164	234	87	247	199	285	285	229	225	197	205.35
Rb	9	5	5	6	11	10	7	10	8	7	11	10	11	16	16	12	9	11	9	13	9.80
Sr	547	519	586	538	627	674	523	644	613	709	382	542	496	479	432	383	567	357	800	827	562.25
Ba	138	104	128	200	155	236	233	196	197	214	182	377	194	270	331	171	112	179	227	220	203.20
Zr	171	148	151	154	203	201	160	185	178	195	124	148	151	140	186	134	127	119	230	231	166.80
Nb	21	16	17	18	26	29	21	28	23	26	15	29	19	28	37	14	14	14	41	43	23.95
Y	21	18	18	21	21	22	19	20	19	21	19	18	22	17	22	18	19	18	20	20	19.65
Ga	22	20	21	21	23	24	22	23	21	22	22	23	24	23	23	22	21	21	23	24	22.25
Th	1.63	1.34	1.49	1.47	2.15	2.01	1.8	1.88	2.06	1.92	1.87	2.66	2.16	2.25	3.44	2.04	2.06	2.16	3.56	3.27	2.16
U	0.48	0.31	0.34	0.27	0.57	0.66	0.49	0.45	0.82	0.51	0.54	0.27	0.52	0.45	0.72	0.61	0.71	0.38	1.25	0.93	0.56
Hf	4.00	3.40	3.80	3.60	4.70	4.60	4.10	4.60	4.40	4.70	3.30	3.90	3.90	3.60	4.70	3.40	3.30	3.20	5.90	5.90	4.15
Ta	1.34	1.08	1.14	1.32	1.67	1.87	2.78	2.13	2.09	2.18	0.91	1.57	1.05	1.71	2.79	1.35	1.30	1.22	3.07	2.72	1.76
Mg no.	0.58	0.62	0.59	0.58	0.60	0.52	0.57	0.53	0.60	0.62	0.51	0.59	0.54	0.61	0.55	0.61	0.62	0.56	0.60	0.59	0.5795

Fe_2O_3* is total iron presented as Fe_2O_3, and Mg no. = molar $Mg/(Mg+Fe^{2+})$ assuming $Fe^{3+}/Fe^{2+} = 0.20$.

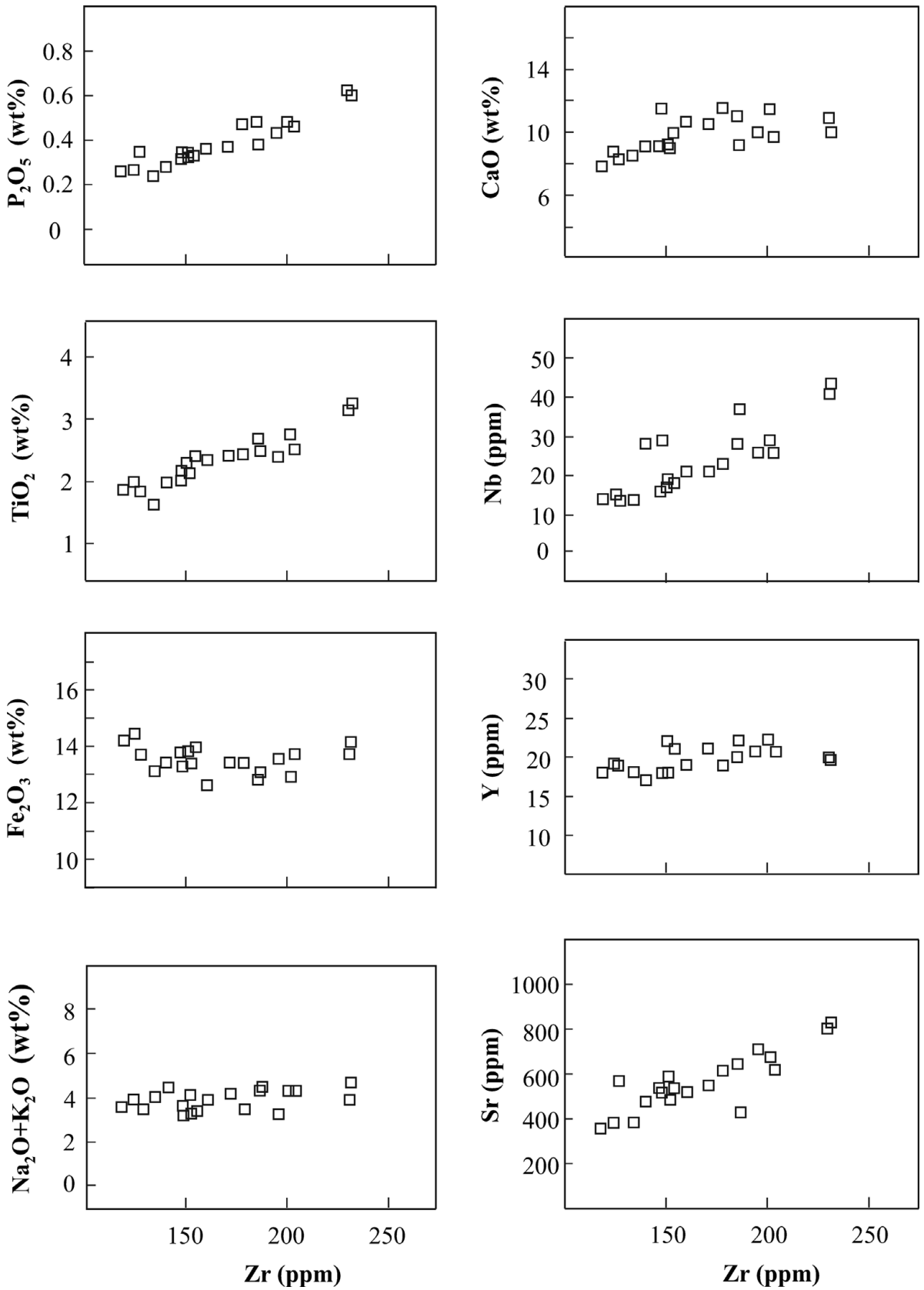

Figure 4. Variations of selected major and trace elements versus Zr within the Tigris volcanic field of northeastern Syria.

the LREEs is a characteristic feature of OIB-type alkali basalts (e.g. Sun & McDonough, 1989; Wittke & Mack, 1993; Abdel-Rahman, 2002): the REE profiles of the Tigris lavas are very similar to those of the St Helena alkali basalts (of Chaffey, Cliff & Wilson (1989) which are typical of high μ (HIMU)-OIB).

Figure 5b, which shows the primitive mantle-normalized incompatible element patterns of the Tigris

https://doi.org/10.1017/S001675681100015X Published online by Cambridge University Press

Table 2. Rare earth element (REE) composition (in ppm) of the Tigris volcanic field, northeastern Syria

Sample	AS07	AS17	AS37	AS57	AS67	AS77	AS104	AS124	AS184	AS194	TG17
La	18.8	15.90	16.90	19.30	25.80	26.40	18.90	23.20	25.40	22.50	14.50
Ce	42.00	35.40	39.00	40.80	55.20	56.70	40.60	51.80	53.80	50.30	32.40
Pr	5.21	4.45	5.03	5.24	6.82	7.06	4.45	6.52	5.75	6.44	3.97
Nd	23.30	20.20	22.10	23.10	29.20	30.60	23.20	26.80	28.90	25.80	17.60
Sm	5.05	4.23	4.76	4.81	6.25	6.48	4.86	6.16	5.63	5.86	4.29
Eu	1.903	1.696	1.915	1.966	2.255	2.357	1.764	2.17	1.922	1.97	1.607
Gd	5.02	4.52	4.70	5.02	5.63	5.64	5.05	5.85	5.70	5.41	4.49
Tb	0.79	0.70	0.76	0.82	0.89	0.91	0.77	0.86	0.81	0.83	0.75
Dy	3.94	3.53	3.82	4.06	4.22	4.50	3.99	4.47	4.19	4.15	3.92
Ho	0.74	0.64	0.69	0.76	0.76	0.82	0.71	0.79	0.71	0.74	0.73
Er	1.79	1.62	1.68	1.82	1.95	2.01	1.90	1.99	1.88	1.87	2.03
Tm	0.247	0.214	0.224	0.267	0.253	0.27	0.256	0.258	0.223	0.234	0.27
Yb	1.47	1.25	1.31	1.48	1.39	1.54	1.62	1.46	1.41	1.30	1.62
Lu	0.222	0.188	0.187	0.202	0.213	0.217	0.223	0.223	0.211	0.20	0.236
∑REE	110.5	94.5	103.1	109.6	140.8	145.5	108.3	132.6	136.5	127.6	88.4

Sample	TG27	TG37	TG47	TG144	TG154	TG164	TG174	SF134	SF27	Ave.
La	22.50	19.10	17.00	23.30	13.80	19.40	15.30	37.40	34.40	21.50
Ce	43.50	41.60	35.20	46.90	28.40	40.70	32.30	76.50	74.20	45.90
Pr	4.99	5.03	4.15	4.94	3.12	4.44	3.48	8.05	8.88	5.40
Nd	20.90	21.20	18.10	25.70	16.70	22.90	18.10	39.40	36.60	24.50
Sm	4.80	5.21	4.30	5.43	3.74	4.81	4.09	7.28	8.10	5.31
Eu	1.715	1.854	1.57	1.756	1.351	1.704	1.454	2.448	2.631	1.90
Gd	4.67	5.04	4.03	5.63	3.94	5.04	4.28	7.12	6.25	5.15
Tb	0.75	0.85	0.68	0.84	0.64	0.76	0.69	0.94	0.95	0.80
Dy	3.84	4.47	3.41	4.45	3.55	3.90	3.85	4.48	4.46	4.06
Ho	0.69	0.81	0.63	0.80	0.66	0.71	0.73	0.77	0.74	0.73
Er	1.80	2.21	1.68	2.15	1.77	1.85	1.93	1.87	1.86	1.88
Tm	0.232	0.29	0.207	0.278	0.24	0.236	0.244	0.217	0.214	0.244
Yb	1.40	1.74	1.30	1.75	1.50	1.46	1.54	1.24	1.25	1.45
Lu	0.196	0.237	0.175	0.258	0.229	0.231	0.227	0.185	0.171	0.212
∑REE	112.0	109.6	92.4	124.2	79.6	108.1	88.2	187.9	180.7	119.0

lavas, indicates that the lavas are enriched in the large ion lithophile elements (LILE: K, Rb, Ba, Th and the LREEs) and the incompatible HFS elements Nb, Zr, and Ti relative to primitive mantle normalizing abundances. The marked depletion of Y and the HREEs in the Tigris lavas reflects that garnet was a residual phase during the partial melting event. According to Pearce *et al*. (1990), melting of 'plume' asthenosphere or lithosphere enriched by small volume melts from the asthenosphere produces 'humped' patterns with Ba, Th and Nb the most enriched elements and the degree of enrichment directly relating to the degree of incompatibility. The Tigris lavas can be interpreted in terms of a mantle source with significant enrichment of asthenospheric melt (see Section 7).

6.c. Rb–Sr and Sm–Nd isotopes

As shown in Table 3, the $^{143}Nd/^{144}Nd$ isotopic compositions of representative samples of the Tigris volcanic field range from 0.512803 ± 1 to 0.512908 ± 1 ($\varepsilon_{Nd} = 3.2$ to 5.3), whereas the $^{87}Sr/^{86}Sr$ ratios range from 0.70327 ± 2 to 0.70403 ± 2. These isotopic compositions are plotted in Figure 6, along with data from other alkali basaltic suites from Jordan, Israel, Lebanon and Syria. Also plotted in this diagram (Fig. 6) are the compositions of various mantle reservoirs (EMI, EMII, HIMU and N-MORB), taken from Hart (1988). It should be noted that EMI ('enriched mantle 1') and EMII ('enriched mantle 2')

Table 3. Sr and Nd isotopic composition of representative samples from the Tigris volcanic field, northeastern Syria

Sample	$^{87}Sr/^{86}Sr$	$^{143}Nd/^{144}Nd$	ε_{Nd}
AS-37	0.70340	0.512881	4.74
AS-77	0.70327	0.512908	5.27
TG-27	0.70390	0.512820	3.55
TG-37	0.70395	0.512803	3.22
TG-47	0.70403	0.512819	3.53

types of OIB may represent the addition of small amounts of subducted sediments: pelagic in the case of EMI and terrigenous in the case of EMII (Weaver, 1991; Hofmann, 1997). HIMU ('high μ') refers to a high $^{238}U/^{204}Pb$ (μ) mantle end-member, and has the lowest $^{87}Sr/^{86}Sr$ of any OIB (Hofmann, 1997), which is thought to be derived from subducted basaltic oceanic crust.

As shown in Figure 6, the Tigris lavas are isotopically similar to the Mesozoic alkali basalts of the Middle East (Laws & Wilson, 1997; Abdel-Rahman, 2002), the Jordanian alkali basalts (Shaw *et al*. 2003), the Lebanese Cenozoic alkali basalts (Abdel-Rahman & Nassar, 2004), the Golan–Galilee alkali basalts (Weinstein *et al*. 2006) and the Euphrates alkali basalts (Lease & Abdel-Rahman, 2008). The investigated lavas also show isotopic compositions similar to OIB-type alkali basalts (e.g. Staudigel *et al*. 1984; Hofmann, 1997), as they exhibit relatively high initial $^{143}Nd/^{144}Nd$ and low initial $^{87}Sr/^{86}Sr$ isotopic ratios, and are thus distinct from EMI-OIB and EMII-OIB (e.g. Weaver,

https://doi.org/10.1017/S001675681100015X Published online by Cambridge University Press

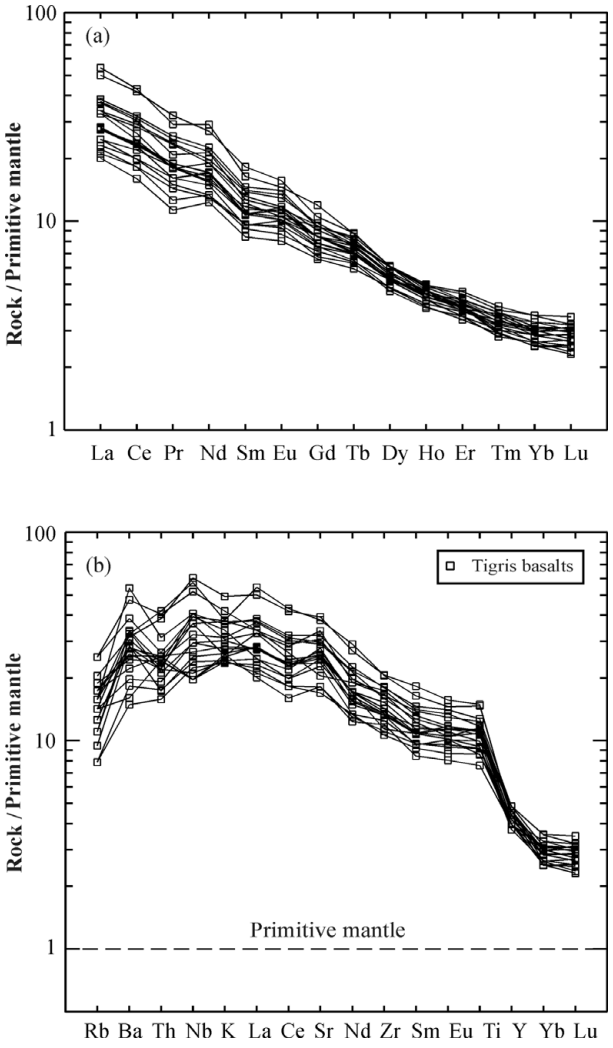

Figure 5. (a) Primitive mantle-normalized rare earth element (REE) patterns of the Tigris volcanic field. (b) Primitive mantle-normalized incompatible element patterns for the Tigris lavas. Normalization values used are from Sun & McDonough (1989).

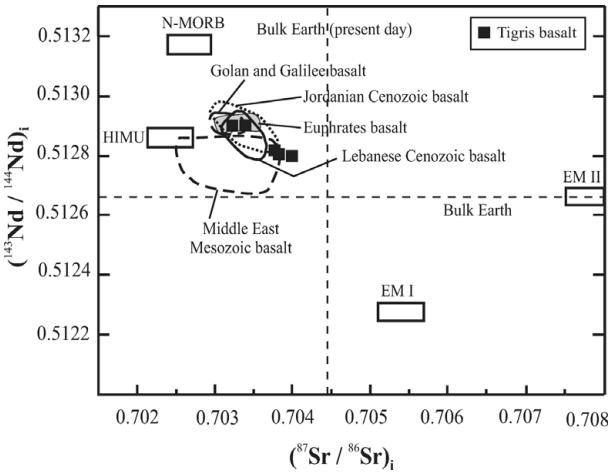

Figure 6. Initial ratios of $^{143}Nd/^{144}Nd$ versus $^{87}Sr/^{86}Sr$ diagram for the Tigris volcanic field of northeastern Syria (squares). Compositions of EMI (enriched mantle 1), EMII (enriched mantle 2), HIMU (high μ) and N-MORB (normal-MORB) are from Hart (1988). Fields for Middle East Mesozoic basalts from Laws & Wilson (1997) and Abdel-Rahman (2002), Jordanian alkali basalts from Shaw *et al*. (2003), Golan–Galilee alkali basalts from Weinstein *et al*. (2006), Lebanese Cenozoic alkali basalts from Abdel-Rahman & Nassar (2004) and Euphrates alkali basalts from Lease & Abdel-Rahman (2008). See text for details.

1991; Wilson, 1993). It should be noted that the Lebanese and the Euphrates lavas were interpreted to represent small-degree partial melts of upper mantle material (Abdel-Rahman & Nassar 2004; Lease & Abdel-Rahman, 2008).

7. Discussion

7.a. Constraints on source region of the Tigris lavas

The presence of garnet as a residual phase in the source region of the Tigris lavas can be inferred from (i) fractionation of the HREEs (McKenzie & O'Nions, 1991) and (ii) the greater than chondritic Dy/Yb ratio (1.57): the Tigris lavas have an average Dy/Yb ratio of 2.8. Variations in some HFS elemental ratios such as Zr/Y versus Zr/Nb (Fig. 7a) indicate that data points of the investigated volcanic rocks plot within or near the fields of plume-related mid-ocean ridge basalt (P-MORB), and HIMU-OIB, as they exhibit relatively lower concentrations of Y, but with higher concentrations of Zr and Nb than transitional-, or normal-MORB (T-MORB or N-MORB; Menzies & Kyle, 1990; Melluso *et al*. 1995). The examined rocks overlap with the Cenozoic alkali basalts of Jordan (after Shaw *et al*. 2003), the Golan–Galilee (Weinstein *et al*. 2006) and the Euphrates region (Lease & Abdel-Rahman, 2008), but exhibit higher Zr/Y ratios than the Lebanese basalts of Abdel-Rahman & Nassar (2004). The Tigris lavas also exhibit elemental ratios (Zr/Nb = 6.96, La/Nb = 1.11, Ba/Th = 94 and Rb/Nb = 0.41, on average) similar to those characteristic of OIB (Weaver, 1991).

Bradshaw & Smith (1994) and Smith *et al*. (1999) have suggested that, since HFS elements (such as Nb) are depleted in the lithospheric mantle relative to the LREEs (e.g. La), high Nb/La ratios (approximately > 1) indicate an OIB-like asthenospheric mantle source for basaltic magmas, and lower ratios (approximately < 0.5) indicate a lithospheric mantle source. The Tigris rocks exhibit Nb/La and La/Yb ratios (1.1 and 16, on average) that are consistent mostly with an asthenospheric mantle (OIB-like) source: data points plot mainly in the field of asthenospheric mantle and near average OIB, but with a few (only 4 out of 20 samples) spilling over into the mixed lithosphere–asthenosphere field (Fig. 7b). This is also consistent with data from the Cenozoic alkali basalts of Jordan, Lebanon, Golan–Galilee and the Euphrates region (after Shaw *et al*. 2003; Abdel-Rahman & Nassar, 2004; Weinstein *et al*. 2006; Lease & Abdel-Rahman, 2008, respectively), as all plot in the field of asthenospheric mantle (Fig. 7b). Thus, trace element and isotopic data (cf. Figs 5–7) suggest that the Tigris lavas have chemical characteristics similar to OIB, and were likely

https://doi.org/10.1017/S001675681100015X Published online by Cambridge University Press

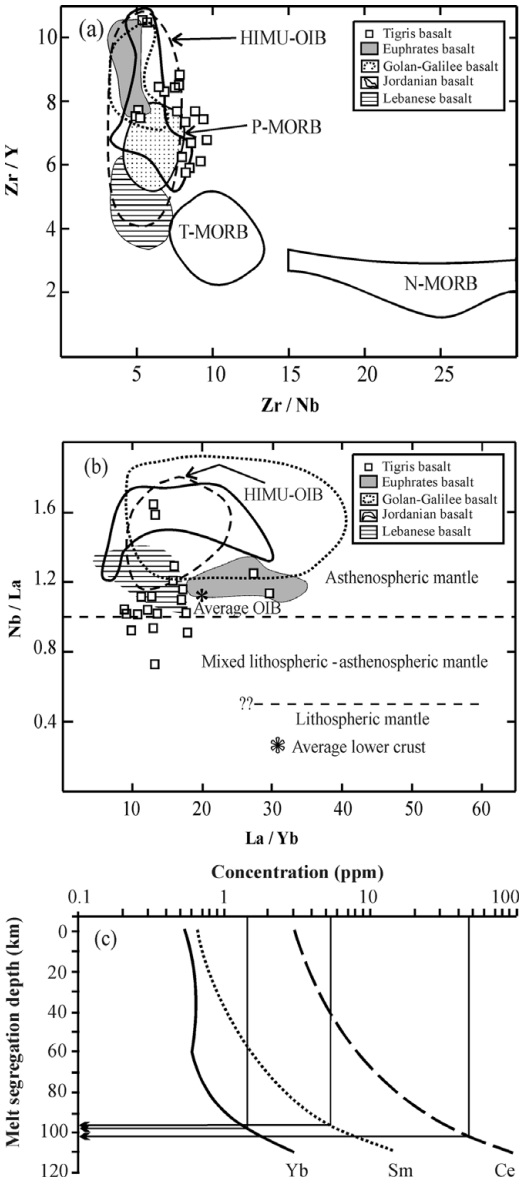

Figure 7. (a) Zr/Y versus Zr/Nb diagram showing that the Tigris volcanic field of northeastern Syria plots near the fields of OIB and HIMU-OIB (taken from Abdel-Rahman, 2002), and near the field of fertile, plume-related MORB (P-MORB). The other fields are transitional-MORB (T-MORB) and normal-MORB (N-MORB) and are taken from Menzies & Kyle (1990). (b) Nb/La versus La/Yb variation diagram. The composition of the Tigris lavas (relatively low La/Yb and high Nb/La) suggests an OIB-like asthenospheric mantle source. Average OIB is after Fitton, James & Leeman (1991), and average lower crust (representing average of six lower crustal granulite xenoliths) is after Chen & Arculus (1995). The field of HIMU-OIB and the dashed lines separating fields of the asthenospheric, lithospheric and mixed mantle are taken from Abdel-Rahman (2002). Fields of Jordanian alkali basalts from Shaw *et al*. (2003); Golan–Galilee alkali basalts from Weinstein *et al*. (2006); Lebanese Cenozoic alkali basalts from Abdel-Rahman & Nassar (2004); Euphrates alkali basalts from Lease & Abdel-Rahman (2008). (c) Model Ce, Sm and Yb concentrations in melts generated by partial melting and ranges of final melt segregation depths (model curves are after Ellam, 1992). The compositions of the Tigris lavas (marked by vertical lines) indicate final melt segregation at depths of 96 to 103 km.

derived from a source within the asthenospheric mantle, near the lithospheric mantle boundary. The relatively uniform $^{143}Nd/^{144}Nd$ ratios ($\varepsilon_{Nd} = 3.2$ to 5.3) within the Tigris volcanic field suggest that its magma was developed by partial melting of an isotopically uniform mantle source.

7.b. Possible depth of melt segregation and role of crustal contamination

McKenzie & O'Nions (1991) and Lassiter, DePaolo & Mahoney (1995) have established that the transition from garnet to spinel peridotite takes place between a depth of about 60 to 80 km for normal mantle and about 80 to 100 km within hot mantle plumes. Based on the study of McKenzie and O'Nions (1991), Ellam (1992) investigated the relationship between the trace element compositions of basalts, variations in thickness of the lithosphere and final depths of melt segregation. Using his method, curves corresponding to the Ce, Sm and Yb concentrations of the Tigris volcanic field (Fig. 7c) indicate a melt segregation depth ranging from about 96 to 103 km (i.e. well within the garnet lherzolite stability field), consistent with an asthenospheric mantle source as indicated above (cf. Fig. 7b).

A number of chemical parameters have been used to assess the degree of contamination that silicate melts may have experienced. For example, basaltic lavas affected by crustal contamination exhibit K/P ratios > 7, La/Ta > 22 and La/Nb > 1.5 (Hart *et al*. 1989). The low values of such elemental ratios in rocks of the Tigris volcanic field (K/P = 4.6; La/Ta = 12; La/Nb = 0.90, on average), along with low ratios of Nb/Y (1.22) and Th/Nb (0.09) suggest that the lavas were not significantly affected by crustal contamination. On the Th/Yb versus Ta/Yb variation diagram of Pearce (1983), the Tigris volcanic rocks plot along the diagonal trend of the mantle spectrum, and away from the trend of crustal contamination (Fig. 8). It should be noted that this alone does not necessarily confirm that no contamination has taken place. However, the relatively low $^{87}Sr/^{86}Sr$ ratios of the Tigris lavas (0.70327 to 0.70403), which could represent mantle source values, along with their low silica values (45.6 wt % SiO_2, on average), further suggest that the magma was subjected to no, or minimal, crustal contamination. As pointed out by Smith *et al*. (1999), the Nd content of most lower crustal xenoliths is too low (usually < 10 ppm) to significantly change Nd-isotopic values without adding 70 % to 85 % lower crustal material. Such large amounts of contamination by crustal material is thermodynamically difficult because a considerable amount of heat is required to assimilate crustal rocks, and the magma would then cool quickly and perhaps 'freeze' in place. Moreover, this would have resulted in the presence of some lower crustal xenoliths within the lava flows, but the Tigris lava flows contain no such crustal xenoliths. Contamination modelling on these rocks produced ambiguous rather than clear results, but the geochemical and field characteristics suggest

https://doi.org/10.1017/S001675681100015X Published online by Cambridge University Press

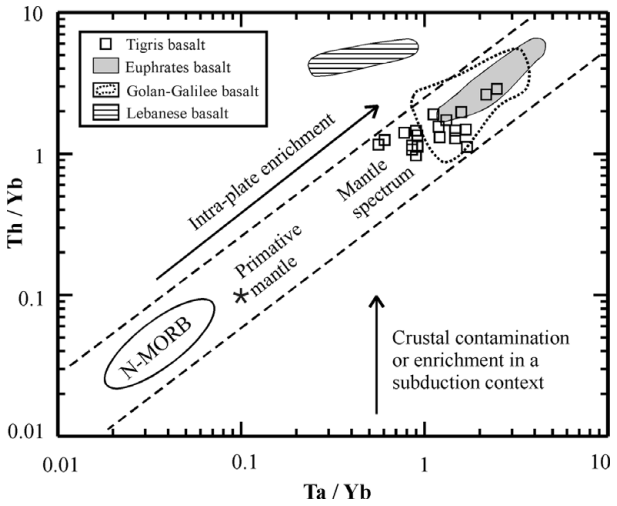

Figure 8. Th/Yb versus Ta/Yb diagram (after Pearce, 1983) showing that the data points of the Tigris volcanic field plot along the diagonal trend of the mantle spectrum, being distinct from the crustal contamination trend. Fields of Golan–Galilee alkali basalts from Weinstein *et al*. (2006); Lebanese Cenozoic alkali basalts from Abdel-Rahman & Nassar (2004); and Euphrates alkali basalts from Lease & Abdel-Rahman (2008).

that the role of crustal contamination during magma evolution has been minimal.

7.c. Petrogenetic considerations: fractional versus batch melting

Various partial melting processes of a multiphase solid assemblage generate magmas. In order to select the proper equations for the petrogenetic modelling of the Tigris lavas, the appropriate process of melting of the mantle source material must first be identified. In fractional melting, the liquid is directly isolated from the system as soon as it is formed and is thereby prevented from further reaction with the crystalline residue. It can be thought of as an infinite number of infinitely small equilibrium fusion events, and large volumes of compositionally distinct magmas can be produced (i.e. liquids of different compositions are formed). Thus, fractional melting is the process by which each infinitesimally small amount of liquid that forms is immediately removed from the source rock.

Kelemen *et al*. (1997) reviewed melting processes beneath ocean spreading ridges; they demonstrated that reactive flow plays an important role, but somewhere in the upwelling, mantle melting must be 'near-fractional', with intergranular porosities less than 1 % and most melt extraction must be in isolated conduits. Kelemen *et al*. (1997) also indicated that not all melting is necessarily near-fractional. Kelemen *et al*. (1997) tested a model in which melting is fractional until 7 wt % melt is extracted, after which an additional 13 % batch melting occurs, thus demonstrating that this model also provides a good fit to the peridotite data they have used. By this, they indicated that there are a rich variety of melt extraction mechanisms (if the amount of reactive porous flow is variable) that produce residues similar to abyssal peridotites. Kelemen *et al*. (1997) stated that ≥ 3 % near-fractional melting is apparently required to account for the abyssal peridotite data.

In sharp contrast to the fractional melting process, equilibrium fusion occurs when the liquid produced on heating continually reacts and re-equilibrates with the crystalline residue (Presnall, 1969). Therefore, when the thermodynamic equilibrium is attained between the melt and the solid, the partitioning of trace elements between melt and solid can be described by equilibrium partition coefficients. This process is often named 'batch partial melting' (Allègre & Minister, 1978). In this process, blobs of magma develop and are then separated from the parent rock. Thus, batch melting refers to the formation of a partial melt in which the liquid remains in equilibrium with the solid residue until it leaves the area as a 'batch' of primary magma.

On the conditions of partial melting (fractional versus batch melting), Gast (1968) demonstrated the difficulty of segregating a small amount or small fractions of liquid from a large volume of residual solid, especially for a small degree of melting (like the case of the Tigris lavas). Some of the physical parameters relevant to this problem are differential buoyancy and surface tension forces. It was also demonstrated that in such a case of a great depth of melting (around 100 km deep), equilibrium between melt and residual solid is normally obtained. Allègre & Minister (1978) indicated that equilibrium partial melting (i.e. batch melting) seems probable for the generation of basaltic magma.

In their study to distinguish between the processes of fractional crystallization, equilibrium (or batch) partial melting and disequilibrium (or fractional) melting, Treuil & Joron (1975) developed the approach of 'magmatophile' elements (such as HREEs, Zr, Hf) and 'hypermagmatophile' elements (such as Ta, Th, La, Ce). They used the diagram La/Sm versus La to demonstrate that during fractional crystallization, data points representing a series of mafic lavas plot along a horizontal line, whereas those produced by batch partial melting plot along a positive trend reflecting gradual increase in La with increasing La/Sm ratios (Fig. 9a). In his study, Loubet (1976), who correlated elements which have similar behaviours and are related by the same mineral phases (see trends shown in the Sr versus Ce diagram, Fig. 9b), ruled out the process of disequilibrium partial melting. Thus, data representing the Tigris volcanic field plot along the batch partial melting trend (Fig. 9). This diagram reflects also that the process of fractional crystallization did not play any significant role during the evolution of the Tigris lavas. In developing their quantitative models for trace elements, a number of authors including Schilling & Winchester (1967), Gast (1968) and Shaw (1970) have used the process of batch partial melting. We have also used the batch partial melting equations in the petrogenetic modelling of the Tigris lavas as given in the next Section.

https://doi.org/10.1017/S001675681100015X Published online by Cambridge University Press

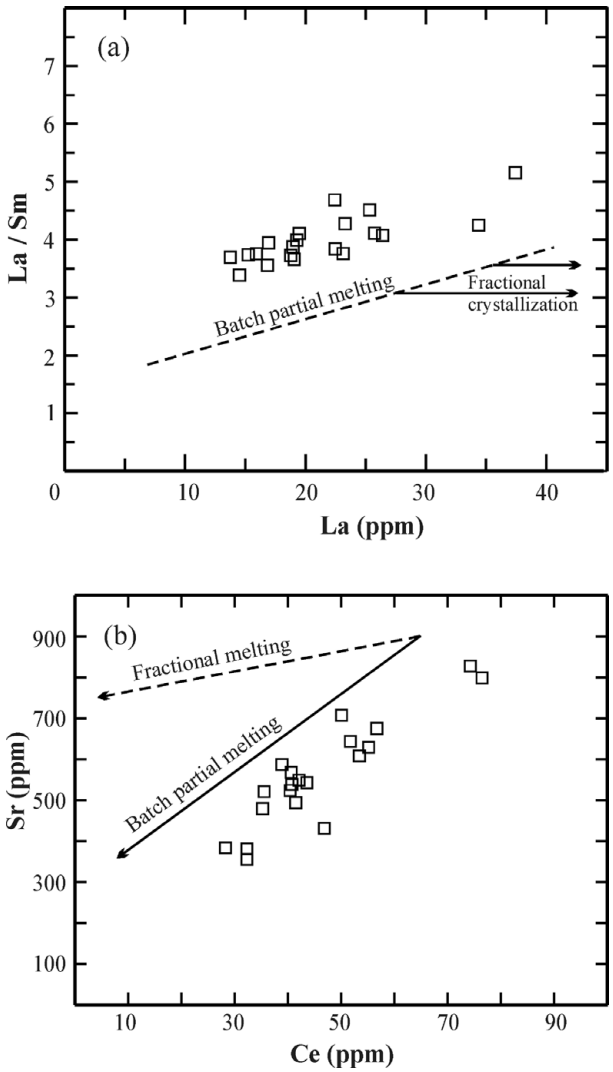

Figure 9. (a) La/Sm versus La diagram (after Truil & Joron, 1975) showing that the data points of the Tigris volcanic field follow a batch partial melting trend. (b) Schematic plot of Sr versus Ce (after Loubet, 1976) showing that the data points of the Tigris volcanic field follow a batch partial melting trend.

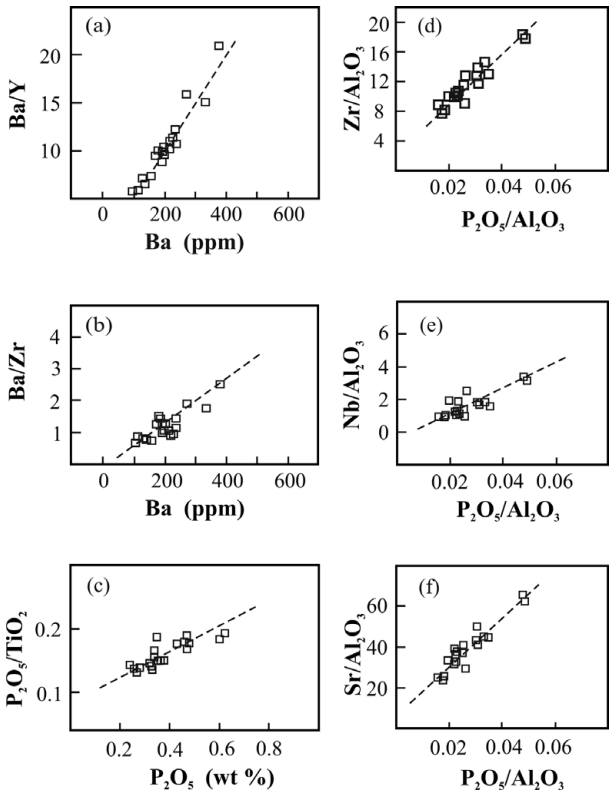

Figure 10. (a, b, c). Plots showing highly/moderately incompatible element ratios versus highly incompatible element concentrations for the Tigris lavas. Zr/Al_2O_3, Nb/Al_2O_3 and Sr/Al_2O_3 versus P_2O_5/Al_2O_3 diagrams (d, e, f, respectively) for the Tigris lavas. See text for details.

7.d. Origin of the Tigris lavas

Several investigations including those of White (1985), Allègre *et al*. (1987), Hart (1988), Weaver (1991), Ellam (1992), Haase (1996), Haase, Stoffers & Garbe-Schönberg (1997), Gibson *et al*. (1997), Abdel-Rahman & Kumarapeli (1999), Frey *et al*. (2000), Gibb & Henderson (2006) and Weinstein *et al*. (2006) show that mafic alkaline lavas are diverse geochemically and form by partial melting of a range of mantle sources. A number of geochemical parameters have been used to assess the role of petrogenetic processes such as fractional crystallization and partial melting in the evolution of mafic lavas. For example, Pankhurst (1977) indicated that during partial melting processes, the highly/moderately incompatible element ratios (such as Ba/Y, Ba/Zr and P_2O_5/TiO_2) are known to decrease with increasing degrees of partial melting, and that partial melting is still by far the most efficient process for fractionating these elements. The linear positive trends between these elemental ratios and the concentrations of the highly incompatible elements (Fig. 10a–c) suggest that partial melting may explain variations in the Tigris lavas. The ratio of an element (X) incompatible during melting to Al_2O_3 (which is usually buffered by residual garnet) typically decreases systematically with increasing degrees of partial melting (Hoernle & Schmincke, 1993). The variations of Zr/Al_2O_3, Nb/Al_2O_3 and Sr/Al_2O_3 versus P_2O_5/Al_2O_3 (Fig. 10d–f) produced linear trends, mostly passing through or near the origin, which is indicative of the significant role of partial melting processes in producing the range of magma chemistry observed in the Tigris volcanic rocks. The available data suggest that the source of these rocks was a fertile, garnet-bearing, asthenospheric mantle.

In order to quantify and assess partial melting as a petrogenetic process, modelling was performed using the batch melting equations of Shaw (1970) and Allègre & Minister (1978), and the calculations were done using two model source compositions. These are a primitive mantle taken from Sun & McDonough (1989) and a mixed (50 % primitive–50 % depleted) mantle source of McKenzie & O'Nions (1991). Spinel, garnet and clinopyroxene were assumed to decrease in abundance linearly with increasing degrees of partial melting, as they are typically consumed at less than

https://doi.org/10.1017/S001675681100015X Published online by Cambridge University Press

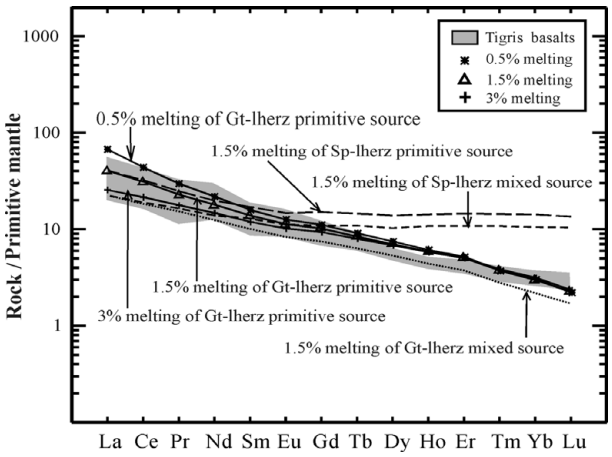

Figure 11. Calculated REE patterns for melts derived by batch partial melting of a primitive mantle composition with REE concentrations from Sun & McDonough (1989) and of a mixed source (50 % primitive/50 % depleted mantle) with REE concentrations from McKenzie & O'Nions (1991). The mantle mineral assemblages and melting proportions used are listed in Table 4. The calculations were made using the Kds of McKenzie & O'Nions (1991), for degrees of partial melting (F) = 0.5 %, 1.5 % and 3 %. Normalization values used are taken from Sun & McDonough (1989). The calculated REE pattern produced by 1.5 % batch melting of a primitive garnet-lherzolite source shows a reasonable fit with that of the average Tigris lavas (Table 4), and falls well within the envelope containing the REE profiles of this volcanic field (shaded grey).

25 % partial melting (McKenzie & O'Nions, 1991; Lassiter, DePaolo & Mahoney, 1995).

Model and melting proportions are given in Table 4, and are in line with those used in other partial melting calculations (e.g. Hanson, 1980; McKenzie & O'Nions, 1991; Witt-Eickschen & Kramm, 1997). Modelling was performed using three different mantle mineral assemblages (spinel lherzolite, garnet lherzolite and spinel–garnet lherzolite) for both a primitive and a mixed source composition. Distribution coefficients (Kds) used are taken from McKenzie & O'Nions (1991). Partial melting calculations were performed for 0.5 %, 1.5 % and 3 % batch partial melting. The results of the modelling (Table 4; Fig. 11) show that melting of a spinel-bearing source overestimates the HREEs, and melting of a mixed source yields much lower LREE concentrations. Thus, neither depleted nor mixed primitive/depleted mantle material represent the mantle source for the Tigris lavas and garnet is a required phase, but possibly with some minor spinel. The REE pattern of the calculated liquid produced by 1.5 % batch partial melting of a fertile, garnet lherzolite (of a primitive mantle composition) produces a reasonable fit, as it closely matches that of the average Tigris lavas (Table 4), and falls well within the envelope containing the REE profiles of these lavas (Fig. 11). Although data for the calculated model liquid and that of the observed melt match closely, Frey, Green & Roy (1978) considered that up to a 15 % difference between calculated and observed melts represented excellent agreement.

7.e. Possible mechanisms of melt generation

Within the various standard tectonic environments of melt generation such as oceanic and continental rifting, leaky transform fault settings and subduction zones, as well as hot spots, several melting mechanisms were introduced. These include (i) shear heating at the base of the lithospheric mantle, (ii) delamination of a thermal boundary layer that may allow decompression of the underlying asthenosphere, and (iii) adiabatic decompression and melting as a result of extension, including transtensional settings.

A number of authors have emphasized the role of shear heating in generating silicate melts. In this mechanism, when the rocks fail (break) as a result of movement of a plate of lithosphere, shear heating is generated and shear melting occurs at the base of the moving lithospheric plate. Using gravitational and bathymetric data, as well as heat flow patterns and anomalous seismic velocities for wave paths through the deep mantle, Shaw & Jackson (1973) demonstrated that the mafic volcanic activity at the ends of the Hawaiian, Tuamoto and Austral linear island chains is not a result of the fortuitous location of thermal plumes, but rather is a consequence of shear melting caused by plate motion. Shaw & Jackson (1973) indicated that as shear melting occurs, a 'thermal feedback' produces more melting, and the residue of unmelted material sinks, creating a 'gravitational anchor' which causes further flow and melting. Several studies have also shown that other magma types such as felsic magmas and alkaline magmas can be generated as a result of shear heating caused by change in plate motion (e.g. de Gruyter & Vogel, 1981; Brown, 1994). According to Giannerini *et al*. (1988), crustal evolution in northeastern Syria during the Plio-Quaternary is marked by a change in the orientation of the regional stress field to a N160°–170°E vertical plane containing σ_1, which induced N80°E-oriented folds along the Palmyra line together with conjugate N40°E sinistral and N100°–110°E dextral strike-slip faults. The sinistral N40°E strike-slip faults controlled the NE movement of the Arabian plate. This tectonic evolution may be related to a slowing of the Arabian plate motion caused by increasing collision in the Zagros–Taurus area (Giannerini *et al*. 1988). The lithospheric mantle of the northern border of the Arabian plate was deformed during and after the collision, leading to the formation of these tectonic features. This could have also provoked the development of shear zones: the equivalent at great depth of detached or transform faults observed in the underlying continental base. Thus, shear heating at the base of the lithospheric mantle of the northern boundary of the Arabian plate, developed as a result of a change in plate motion as the Arabian plate moved in a more easterly direction during the Plio-Quaternary (as reflected by the sinistral motion in the Palmyrian area; Giannerini *et al*. 1988) could represent a viable mechanism providing heat necessary for partial fusion and magma generation.

https://doi.org/10.1017/S001675681100015X Published online by Cambridge University Press

Table 4. Model parameters and results of batch partial melting calculations using various mineralogical and chemical compositions of primitive and mixed mantle sources

							Starting mode			Melt mode									
						Phase	a	b	c	a	b	c							
						Olivine	0.570	0.550	0.55	0.15	0.05	0.15							
						Opx	0.235	0.220	0.22	0.15	0.05	0.15							
						Cpx	0.160	0.160	0.16	0.35	0.30	0.35							
						Garnet	0.000	0.035	0.07	0.00	0.30	0.35							
						Spinel	0.035	0.035	0.00	0.35	0.30	0.00							
REE	1	2	3	4	5	6	7	8	9	10	11	12	13	14	15	16	17	18	19
La	25.93	15.52	9.69	25.38	15.32	9.61	25.39	15.32	9.61	47.13	28.21	17.61	46.14	27.85	17.46	46.15	17.47	27.86	21.50
Ce	48.60	33.74	23.13	47.14	33.03	22.80	46.38	32.69	22.66	81.31	56.44	38.69	78.86	55.26	38.14	77.59	37.91	54.69	45.90
Pr	5.92	4.52	3.34	5.59	4.34	3.25	5.35	4.20	3.17	9.00	6.88	5.08	8.51	6.60	4.946	8.13	4.83	6.39	5.40
Nd	23.27	18.98	14.86	21.75	18.04	14.30	20.51	17.18	13.82	33.24	27.10	21.23	31.07	25.71	20.43	29.30	19.74	24.54	24.50
Sm	6.55	5.54	4.50	5.72	4.98	4.16	5.08	4.50	3.83	8.95	7.57	6.15	7.82	6.80	5.68	6.95	5.24	6.15	5.31
Eu	2.10	1.83	1.52	1.78	1.59	1.38	1.54	1.40	1.24	2.87	2.49	2.08	2.43	2.18	1.88	2.10	1.69	1.92	1.90
Gd	7.62	6.60	5.50	5.92	5.37	4.71	4.82	4.47	4.02	10.38	8.98	7.48	8.06	7.31	6.42	6.56	5.48	6.08	5.15
Tb	1.35	1.18	0.99	0.957	0.88	0.79	0.73	0.69	0.64	1.80	1.57	1.32	1.27	1.18	1.06	0.97	0.85	0.92	0.80
Dy	8.59	7.55	6.395	5.534	5.22	4.82	4.04	3.89	3.69	11.57	10.17	8.60	7.45	7.03	6.49	5.44	4.97	5.24	4.06
Ho	2.03	1.77	1.49	1.11	1.07	1.01	0.75	0.74	0.71	2.67	2.33	1.96	1.46	1.40	1.32	0.99	0.94	0.97	0.73
Er	5.92	5.16	4.33	2.82	2.75	2.66	1.83	1.81	1.78	7.90	6.90	5.79	3.77	3.68	3.55	2.44	2.38	2.42	1.88
Tm	0.91	0.79	0.66	0.34	0.34	0.34	0.21	0.21	0.21	1.20	1.05	0.88	0.45	0.45	0.45	0.27	0.28	0.28	0.24
Yb	5.80	5.07	4.27	1.83	1.86	1.90	1.07	1.08	1.11	7.95	6.95	5.85	2.51	2.55	2.61	1.46	1.52	1.49	1.45
Lu	0.86	0.76	0.64	0.22	0.23	0.24	0.12	0.13	0.13	1.146	1.00	0.85	0.29	0.30	0.32	0.16	0.17	0.17	0.21

Calculated melts produced by 0.5 %, 1.5 % and 3 % batch partial melting are no. 1 to no. 18; no. 19 is the measured average REE concentration of the Tigris lavas. The starting mode, melt mode and mantle source type used to produce each of the calculated melts are as follows:
Melt nos. 1–3: starting mode a, melt mode a, mixed source, for 0.5, 1.5 and 3.0 % melting, respectively;
nos. 4–6: starting mode b, melt mode b, mixed source, for 0.5, 1.5 and 3.0 % melting, respectively;
nos. 7–9: starting mode c, melt mode c, mixed source, for 0.5, 1.5 and 3.0 % melting, respectively;
Melt nos. 10–12: starting mode a, melt mode a, primitive source, for 0.5, 1.5, and 3.0 % melting, respectively;
nos. 13–15; starting mode b, melt mode b, primitive source, for 0.5, 1.5 and 3.0 % melting, respectively;
nos. 16–18: starting mode c, melt mode c, primitive source, for 0.5, 3 and 1.5 % melting, respectively.
The composition of the calculated melt no. 18 (produced by 1.5 % melting of garnet lherzolite of a primitive mantle source) closely matches that of the measured average composition of the Tigris lavas (no. 19). See text for details.

In their study of volcanism in East Anatolia, Pearce *et al*. (1990) indicated that perturbation of the thickened lithosphere by delamination of the thermal boundary layer, perhaps coupled with local stretching associated with pull-apart basins on strike-slip fault systems, is sufficient to generate melt. Unlike the case of East Anatolia, Lustrino & Sharkov (2006) in their study of the Neogene volcanic activity of western Syria proposed that the transition from strongly compressive to transtensional stresses may have allowed for partial melting as a consequence of mantle decompression.

Although geochemical data cannot differentiate between the various processes of magma generation in this region, the most generally applicable one is the adiabatic decompression of an ascending solid diapir. The diapir rises because it experiences a positive buoyancy force deriving from either compositional or thermal effects. As demonstrated by Spera (1980), when the temperature–depth trajectory of the adiabatically ascending crystalline diapir intersects the peridotite solidus, partial fusion begins. The energy necessary for fusion comes from the heat content of the diapir. After partial fusion has begun, there will be a tendency for melt to segregate. A large blob of magma may be imagined to rise through the relatively cool lithosphere by softening a thin rind of wall rock, causing it to flow past the magma (Spera, 1980). The effective viscosity of the wall rock is significantly lowered in response to transient heating and partial melting. Thus, the process of adiabatic decompression and melting has been known to be very efficient in magma generation, and it represents a more likely process in providing heat necessary for the production of the Tigris magma. Sawaf *et al*. (1993) used seismic reflection data to show that Quaternary volcanism in northeastern Syria occurred above some of the deeper penetrating faults.

8. Conclusions

Large exposures of Quaternary mafic–ultramafic lavas (covering 1750 km^2), forming the Tigris volcanic field of northeastern Syria, represent the northernmost tip of the Cenozoic volcanic province of the Middle East. This volcanic field occurs between the Euphrates graben and the Bitlis–Zagros collision suture that forms the Arabian/Eurasian plate boundary. The rocks are mostly phyric, consisting of about 50–55 vol. % labradorite, 35 % clinopyroxene, 10–15 % olivine and opaque phases. The Tigris lavas are compositionally restricted to basanites and alkali basalts, having a narrow range of major element compositions (SiO_2, 42.2–48.2 wt %; MgO, 5.7–9.0 wt %), are alkaline in nature, and are enriched in Ti (1.7–3.2 wt % TiO_2), Zr (119–231 ppm), Nb (14–43 ppm) and Y (17–22 ppm). These features reflect strong affinities to OIB. The primitive mantle-normalized patterns are strongly fractionated ($(La/Yb)_N = 10.6$) indicative of a garnet-bearing source. The $^{143}Nd/^{144}Nd$ isotopic composition of the Tigris lavas ranges from 0.512803 to 0.512908, and $^{87}Sr/^{86}Sr$ from 0.70327 to 0.70403 ($\varepsilon_{Nd} = 3.2$ to 5.3). Petrogenetic modelling along with the overall chemical and petrological characteristics are consistent with the generation of the Tigris magma by a small degree of batch partial melting ($F = 1.5$ %) of a deep, garnet-facies, asthenospheric mantle source, possibly containing a minor spinel component. The magmas probably experienced very rapid ascent, with minimal interaction with the crust and little or no crustal contamination as confirmed by various elemental ratios such as K/P (4.6, on average), La/Ta (12), La/Nb (0.90), Nb/Y (1.22) and Th/Nb (0.09), and the low silica values (45.6 wt % SiO_2, on average). Shear heating at the base of the lithospheric mantle of the northern boundary of the Arabian plate, developed as a result of a change in plate motion as the Arabian plate moved in a more easterly direction during the Plio-Quaternary could represent a possible cause providing the heat necessary for partial fusion and magma generation. Adiabatic decompression and melting represents a more likely process for the generation of the Tigris magma. Further detailed investigations on products of Cenozoic volcanism in other parts of the Middle East are warranted, in view of their significance in evaluating regional tectonic regimes, Cenozoic mantle dynamics and crustal evolution of the eastern Mediterranean region.

Acknowledgements. The collaboration of Roger Laurent (Laval University, Québec) was essential in this study. We thank Alan Dickin at MacMaster University, Ontario, for isotope analysis work. We acknowledge the help of A. A. Turkmani, Ministry of Petroleum and Mineral Resources of Syria, during the field work, as well as that of Muawia Barazangi and Graham Brew at Cornell University and Michel Delaloye of the University of Geneva. The technical support provided by M. Ijreiss of the American University of Beirut (Lebanon) is appreciated. This work was part of a larger research project made possible by grants from the Fonds pour la formation de chercheurs et l'aide à la recherche (Québec) and the Conseil de recherches en sciences humaines du Canada. Helpful reviews and valuable comments provided by John Maclennan, an anonymous referee and by the editor (Mark Allen) improved this contribution.

References

ABDEL-RAHMAN, A. M. 2002. Mesozoic volcanism in the Middle East: geochemical, isotopic and petrogenetic evolution of extension-related alkali basalts from central Lebanon. *Geological Magazine* **139**, 621–40.

ABDEL-RAHMAN, A. M. & KUMARAPELI, P. S. 1999. Geochemistry and petrogenesis of the Tibbit Hill metavolcanic suite of the Appalachian Fold Belt, Quebec-Vermont: a plume-related and fractionated assemblage. *American Journal of Science* **299**, 210–37.

ABDEL-RAHMAN, A. M. & NASSAR, P. E. 2004. Cenozoic volcanism in the Middle East: petrogenesis of alkali basalts from northern Lebanon. *Geological Magazine* **141**, 545–63.

ALLÈGRE, C. J., HAMELIN, B., PROVOST, A. & DUPRÉ, B. 1987. Topology in isotopic multispace and origin of

https://doi.org/10.1017/S001675681100015X Published online by Cambridge University Press

mantle chemical heterogeneities. *Earth and Planetary Science Letters* **81**, 319–37.

ALLÈGRE, C. J. & MINSTER, J. F. 1978. Quantitative models of trace element behavior in magmatic processes. *Earth and Planetary Science Letters* **38**, 1–25.

BAKER, J. A., CHAZOT, G., MENZIES, M. A. & THIRLWALL, M. F. 1998. Metasomatism of the shallow mantle beneath Yemen by the Afar plume – implications for mantle plumes, flood volcanism, and intraplate volcanism. *Geology* **26**, 431–4.

BAKER, J. A., MENZIES, M. A., THIRLWALL, M. F. & MACPHERSON, C. J. 1997. Petrogenesis of Quaternary intraplate volcanism, Sana'a, Yemen: implications for plume-lithosphere interaction and polybaric melt hybridization. *Journal of Petrology* **38**, 1359–90.

BAKER, J. A., THIRLWALL, M. F. & MENZIES, M. A. 1996. Sr-Nd-Pb isotopic and trace element evidence for crustal contamination of plume-derived flood basalts: Oligocene flood volcanism in western Yemen. *Geochimica et Cosmochimica Acta* **60**, 2559–81.

BALDRIDGE, W. S., EYAL, Y., BARTOV, Y., STEINITZ, G. & EYAL, M. 1991. Miocene magmatism of Sinai related to the opening of the Red Sea. *Tectonophysics* **197**, 181–201.

BARBERI, F., FERRARA, G., SANTACROCE, R., TREUIL, M. & VARET, J. 1975. A transitional basalt-pantellerite sequence of fractional crystallization: the Boina center (Afar rift, Ethiopia). *Journal of Petrology* **16**, 22–56.

BARRAT, J. A., FOURCADE, S., JAHN, B. M., CHEMINÈE, J. L. & CAPDEVILA, R. 1998. Isotope (Sr, Nd, Pb, O) and trace element geochemistry of volcanics from the Erta' Ale range (Ethiopia). *Journal of Volcanology and Geothermal Research* **80**, 85–100.

BERTRAND, H., CHAZOT, G., BLICHERT-TOFT, J. & THORAL, S. 2003. Implications of widespread high–μ volcanism on the Arabian Plate for Afar mantle plume and lithosphere composition. *Chemical Geology* **198**, 47–61.

BRADSHAW, T. K. & SMITH, E. I. 1994. Polygenetic Quaternary volcanism at Crater Flat, Nevada. *Journal of Volcanology and Geothermal Research* **63**, 165–82.

BROWN, M. 1994. The generation, segregation, ascent and emplacement of granite magma: the migmatite-to-crustally-derived granite connection in thickened orogens. *Earth Science Reviews* **36**, 83–130.

CAMP, V. E. & ROOBOL, M. J. 1989. The Arabian continental alkali basalt province: Part I. Evolution of Harrat Rahat, Kingdom of Saudi Arabia. *Geological Society of America Bulletin* **101**, 71–95.

CAMP, V. E. & ROOBOL, M. J. 1992. Upwelling asthenosphere beneath western Arabia and its regional implications. *Journal of Geophysical Research* **97B**, 15255–71.

CAMP, V. E., ROOBOL, M. J. & HOOPER, P. R. 1992. The Arabian continental alkali basalt province: Part III. Evolution of Harrat Kishb, Kingdom of Saudi Arabia. *Geological Society of America Bulletin* **104**, 379–96.

CHAFFEY, D. J., CLIFF, R. A. & WILSON, B. M. 1989. Characterization of the St Helena magma source. In *Magmatism in the Ocean Basins* (eds A. D. Saunders & M. J. Norry), pp. 257–76. Geological Society of London, Special Publication no. 42.

CHEN, W. & ARCULUS, R. J. 1995. Geochemical and isotopic characteristics of lower crustal xenoliths, San Francisco Volcanic Field, Arizona, U.S.A. *Lithos* **36**, 203–325.

DE GRUYTER, P. & VOGEL, T. A. 1981. A model for the origin of the alkaline complexes of Egypt. *Nature* **291**, 571–4.

DUBERTRET, L. 1955. Carte Geologique du, Liban aux 1/200,000, avec notice explicative. Ministire des Travaux Public, Beyrouth. 74 pp.

EBINGER, C. J. & SLEEP, N. H. 1998. Cenozoic magmatism throughout east Africa resulting from impact of a single plume. *Nature* **395**, 788–91.

ELLAM, R. M. 1992. Lithospheric thickness as a control on basalt geochemistry. *Geology* **20**, 153–6.

FITTON, J. G., JAMES, D. & LEEMAN, W. P. 1991. Basic magmatism associated with Late Cenozoic extension in the western United States: compositional variations in space and time. *Journal of Geophysical Research* **96**, 13693–712.

FREY, F. A., CLAGUE, D., MAHONEY, J. J. & SINTON, J. M. 2000. Volcanism at the edge of the Hawaiian plume: petrogenesis of submarine alkalic lavas from the North Arch Volcanic Field. *Journal of Petrology* **41**, 667–91.

FREY, F. A., GREEN, D. H. & ROY, S. D. 1978. Integrated models of basalt petrogenesis: a study of quartz tholeiites to olivine melilites from southeastern Australia utilizing geochemical and experimental data. *Journal of Petrology* **19**, 463–513.

FURMAN, T., BRYCE, J. G., KARSON, J. & IOTTI, A. 2004. East African Rift System (EARS) plume structure: insights from Quaternary mafic lavas of Turkana, Kenya. *Journal of Petrology* **45**, 1069–88.

FURMAN, T., KALETA, K. M., BRYCE, J. G. & HANAN, B. B. 2006. Tertiary mafic lavas of Turkana, Kenya: constraints on East African plume structure and the occurrence of high–μ volcanism in Africa. *Journal of Petrology* **47**, 1221–44.

GARFUNKEL, Z. 1989. Tectonic setting of Phanerozoic magmatism in Israel. *Israel Journal of Earth Sciences* **38**, 51–74.

GAST, P. W. 1968. Trace element fractionation and the origin of tholeiitic and calc-alkaline magma types. *Geochimica et Cosmochimica Acta* **32**, 1057–86.

GEORGE, R. & ROGERS, N. 2002. Plume dynamics beneath the African plate inferred from the geochemistry of the Tertiary basalts of southern Ethiopia. *Contributions to Mineralogy and Petrology* **144**, 286–304.

GIANNÉRINI, G., CAMPREDON, R., FÉRAUD, G. & ABOU ZAKHEM, B. 1988. Déformations intraplaques et volcanisme associé: exemple de la bordure NW de la plaque Arabique au Cénozoïque. *Bulletin de la Société géologique de France* **8**, 937–47.

GIBB, F. G. F. & HENDERSON, C. M. B. 2006. Chemistry of the Shiant Isles main sill, NW Scotland, and wider implications for the petrogenesis of mafic sills. *Journal of Petrology* **47**, 191–230.

GIBSON, S. A., THOMPSON, R. N., WESKA, R. K., DICKIN, A. P. & LEONARDOS, O. H. 1997. Late Cretaceous rift-related upwelling and melting of the Trinidad starting mantle plume head beneath western Brazil. *Contributions to Mineralogy and Petrology* **126**, 303–14.

HANSON, G. N. 1980. Rare earth elements in petrogenetic studies of igneous systems. *Annual Reviews in Earth Sciences* **8**, 371–406.

HART, S. R. 1988. Heterogeneous mantle domains signatures, genesis and mixing chronologies. *Earth and Planetary Science Letters* **90**, 273–96.

HART, W. K., WOLDE, G. C., WALTER, R. C. & MERTZMAN, S. A. 1989. Basaltic volcanism in Ethiopia: constraints on continental rifting and mantle interactions. *Journal of Geophysical Research* **94**, 7731–48.

HAASE, K. M. 1996. The relationship between the age of the lithosphere and the composition of oceanic magmas:

constraints on partial melting, mantle sources, and the thermal structure of the plates. *Earth and Planetary Science Letters* **144**, 75–92.

HAASE, K. M., STOFFERS, P. & GARBE-SCHÖNBERG, C. D. 1997. The petrogenetic evolution of lavas from Easter Island and neighbouring seamounts, near-ridge hotspot volcanoes in the SE Pacific. *Journal of Petrology* **38**, 785–813.

HOERNLE, K. & SCHMINCKE, H. U. 1993. The role of partial melting in the 15 Ma geochemical erosion of Gran Canaria: a blob model for the Canary hotspot. *Journal of Petrology* **34**, 599–626.

HOFMANN, A. W. 1997. Mantle geochemistry: the message from oceanic volcanism. *Nature* **385**, 219–29.

KELEMEN, P. B., HIRTH, G., SHIMIZU, N., SPIEGELMAN, M. & DICK, H. J. B. 1997. A review of melt migration processes in the adiabatically upwelling mantle beneath oceanic spreading ridges. *Philosophical Transactions of the Royal Society of London* **A-355**, 283–318.

LASSITER, J. C., DEPAOLO, D. J. & MAHONEY, J. J. 1995. Geochemistry of the Wrangellia Flood Basalt Province: implications for the role of continental and oceanic lithosphere in flood basalt genesis. *Journal of Petrology* **36**, 983–1009.

LAWS, E. D. & WILSON, M. 1997. Tectonics and magmatism associated with Mesozoic passive continental margin development in the Middle East. *Journal of the Geological Society, London* **154**, 757–60.

LEASE, N. A. & ABDEL-RAHMAN, A. M. 2008. The Euphrates volcanic field, northeastern Syria: petrogenesis of Cenozoic basanites and alkali basalts. *Geological Magazine* **145**, 685–701.

LE BAS, M. J. & STRECKEISEN, A. L. 1991. The IUGS systematics of igneous rocks. *Journal of the Geological Society, London* **148**, 825–33.

LOUBET, M. 1976. Géochimie des terres rares dans les massifs de péridotites dits de 'haute température': évolution du manteau terrestre. Published Thèse de Doctorat d'ètat, Université de Paris VII, Paris. 380 pp.

LUSTRINO, M. & SHARKOV, E. 2006. Neogene volcanic activity of western Syria and its relationship with Arabian plate kinematics. *Journal of Geodynamics* **42**, 140–58.

LYBERIS, N., YURUR, T., CHOROWICZ, J., KASAPOGLU, E. & GUNDOGDU, N. 1992. The East Anatolian Fault: an oblique collisional belt. In *The Afro-Arabian Rift System* (ed. R. Altherr). *Tectonophysics* **204**, 1–15.

MCKENZIE, D. P. & O'NIONS, R. K. 1991. Partial melting distributions from inversion of rare earth element concentrations. *Journal of Petrology* **32**, 1021–91.

MELLUSO, L., BECCALUVA, L., BROTZU, P., GREGNANIN, A., GUPTA, A. K., MORBIDELLI, L. & TRAVERSA, G. 1995. Constraints on the mantle sources of the Deccan Traps from the petrology and geochemistry of the basalts of Gujarat State (Western India). *Journal of Petrology* **36**, 1393–432.

MENZIES, M. A. & KYLE, R. 1990. Continental volcanism: a crust-mantle probe. In *Continental Mantle* (ed. M. A. Menzies), pp. 157–77. Oxford: Oxford Science Publishers.

MESCHEDE, M. A. 1986. A method of discriminating between different types of mid ocean ridge basalts and continental tholeiites with the Nb-Zr-Y diagram. *Chemical Geology* **56**, 207–18.

MOHR, P. 1983. Ethiopian flood basalt province. *Nature* **303**, 577–84.

MOUTY, M., DELALOYE, M., FONTIGNIE, D., PISKIN, O. & WAGNER, J.-J. 1992. The volcanic activity in Syria and Lebanon between Jurassic and actual. *Schweizerische Mineralogische Und Petrografische Mitteilungen* **72**, 91–105.

NICHOLSON, H. & LATIN, D. 1992. Olivine tholeiites from Krafla, Iceland: evidence for variation in melt fraction within a plume. *Journal of Petrology* **33**, 1105–24.

NOTSU, K., FUJITANI, T., UI, T., MATSUDA, J. & ERCAN, T. 1995. Geochemical features of collision-related volcanic rocks in central and eastern Anatolia, Turkey. *Journal of Volcanology and Geothermal Research* **64**, 171–92.

PANKHURST, R. J. 1977. Open system fractionation and incompatible element variations in basalts. *Nature* **268**, 36–8.

PEARCE, J. A. 1983. Role of the sub-continental lithosphere in magma genesis at active continental margins. In *Continental Basalts and Mantle Xenoliths* (eds C. J. Hawkesworth & M. J. Norry), pp. 230–49. Cheshire, UK: Shiva Publishing Ltd.

PEARCE, J. A., BENDER, J. F., DE LONG, S. E., KIDD, W. S. F., LOW, P. J., GÜNER, Y., SAROGLU, F., YILMAZ, Y., MOORBATH, S. & MITCHELL, J. G. 1990. Genesis of collision volcanism in Eastern Anatolia, Turkey. *Journal of Volcanology and Geothermal Research* **44**, 189–229.

PEARCE, J. A. & NORRY, M. J. 1979. Petrogenetic implications of Ti, Zr, Y, and Nb variations in volcanic rocks. *Contributions to Mineralogy and Petrology* **69**, 33–47.

PIK, R., DENIEL, C., COULON, C., YIRGU, G. & MARTY, B. 1999. Isotopic and trace element signatures of Ethiopian flood basalts; evidence for plume-lithosphere interactions. *Geochimica et Cosmochimica Acta* **63**, 2263–79.

PONIKAROV, V. P. (ed.) 1967. The Geology of Syria: Explanatory Notes on the Geological Map of Syria, Scale 1:5 000 000, Part I, Stratigraphy, Igneous Rocks and Tectonics. Damascus, Syria: Ministry of Industry, 88 pp.

PRESNALL, D. C. 1969. The geometrical analysis of partial fusion. *American Journal of Science* **267**, 1178–94.

RICHARD, P., SHIMIZU, N. & ALLÈGRE, C. J. 1976. $^{143}Nd/^{144}Nd$, a natural tracer: an application to oceanic basalts. *Earth and Planetary Science Letters* **31**, 269–78.

SAWAF, T., AL-SAAD, D., GEBRAN, A., BARAZANGI, M., BEST, J. A. & CHAIMOV, T. 1993. Stratigraphy and structure of eastern Syria across the Euphrates depression. *Tectonophysics* **220**, 267–81.

SCHILLING, J. G. & WINCHESTER, J. W. 1967. Rare-earth fractionation and magmatic processes. In *Mantles of Earth and Terrestrial Planets* (ed. S. K. Runcorn), pp. 267–83. New York, N. Y.: Interscience.

SHAW, D. M. 1970. Trace element fractionation during anatexis. *Geochimica et Cosmochimica Acta* **34**, 237–343.

SHAW, J. E., BAKER, J. A., MENZIES, M. A., THIRLWALL, M. F. & IBRAHIM, K. M. 2003. Petrogenesis of the largest intraplate volcanic field on the Arabian Plate (Jordan): a mixed lithosphere-asthenosphere source activated by lithospheric extension. *Journal of Petrology* **44**, 1657–79.

SHAW, H. R. & JACKSON, E. D. 1973. Linear island chains in the Pacific; results of thermal plumes or gravitational anchors? *Journal of Geophysical Research* **78**, 8634–52.

SMITH, E. I., SÁNCHEZ, A., WALKER, J. D. & WANG, K. 1999. Geochemistry of mafic magmas in the Hurricane Volcanic Field, Utah: implications for small- and large-scale chemical variability of the lithospheric mantle. *Journal of Geology* **107**, 433–48.

SPERA, F. J. 1980. Aspects of magma transport. In *Physics of Magmatic Processes* (ed. R. B. Hargraves), pp. 265–324. Princeton, New Jersey: Princeton University Press.

STAUDIGEL, H., ZINDLER, A., HART, S. R., LESLIE, C. Y. & CLAGUE, D. 1984. The isotope systematics of a juvenile intra-plate volcano: Pb, Nd and Sr isotope ratios of basalts from Loihi Seamount, Hawaii. *Earth and Planetary Science Letters* **69**, 13–29.

STEWART, K. & ROGERS, N. 1996. Mantle plume and lithosphere contributions to basalts from southern Ethiopia. *Earth and Planetary Science Letters* **139**, 195–211.

SUN, S. & MCDONOUGH, W. F. 1989. Chemical and isotopic systematics of oceanic basalts: implications for mantle composition and processes. In *Magmatism in the Ocean Basins* (eds A. D. Saunders & M. J. Norry), pp. 313–45. Geological Society of London, Special Publication no. 42.

TREUIL, M. & JORON, J. M. 1975. Utilisation des éléments hygromagmatophiles pour la simplification de la modélisation quantitative des processus magmatiques. Exemples de l'Afar et de la dorsade médioatlantique. *Société Italiana Mineralogié et Petrologié*, **31**, 125–42.

WEAVER, B. L. 1991. Trace element evidence for the origin of ocean-island basalts. *Geology* **19**, 123–6.

WEINSTEIN, Y., NAVON, O., ALTHERR, R. & STEIN, M. 2006. The role of lithospheric mantle heterogeneity in the generation of Plio-Pleistocene alkali basaltic suites from Harrat Ash Shaam (Israel). *Journal of Petrology* **47**, 1017–50.

WHITE, W. M. 1985. Sources of oceanic basalts: radiogenic isotopic evidence. *Geology* **13**, 115–118.

WHITE, R. S. & MCKENZIE, D. P. 1989. Magmatism at rift zones: the generation of volcanic continental margins and flood basalts. *Journal of Geophysical Research* **94**, 7685–730.

WILSON, M. 1993. Geochemical signatures of oceanic and continental basalts: a key to mantle dynamics? *Journal of the Geological Society, London* **150**, 977–90.

WITT-EICKSCHEN, G. & KRAMM, U. 1997. Mantle upwelling and metasomatism beneath central Europe: geochemical and isotopic constraints from mantle xenoliths from the Rhon (Germany). *Journal of Petrology* **38**, 479–93.

WITTKE, J. H. & MACK, L. E. 1993. OIB-like mantle source for continental alkaline rocks of the Balcones province, Texas: trace element and isotopic evidence. *Journal of Geology* **101**, 333–44.

https://doi.org/10.1017/S001675681100015X Published online by Cambridge University Press